Analysis, Design and Testing of a Wind Tunnel Model to Validate Fiber-Optic Shape Sensing Systems

Ryan M. Montero

Thesis submitted to the faculty of the Virginia Polytechnic Institute and State University in partial fulfillment of the requirements for the degree of

Master of Science

In

Aerospace Engineering

Joseph A. Schetz, Chair

Rakesh K. Kapania

William J. Devenport

April 29, 2013

Blacksburg, VA

Keywords: flexible wing, shape sensing wing, aeroelastics

Analysis, Design, and Testing of a Wing Tunnel Model

Ryan M. Montero

ABSTRACT

The ability to collect valuable data concerning the stress, strains, and shape profiles of aircraft and aircraft components during flight is important to fields such as structural health monitoring, gust alleviation, and flutter control. A research interest in the form of a NASA Phase I SBIR called for possible systems that would be able to take accurate shape sensing data on a flexible wing aircraft. In a joint venture between Luna Technologies Inc. and Virginia Polytechnic Institute and State University a flexible wing wind tunnel model was designed and constructed as a test article for the Luna Technologies Inc. fiber optic shape sensing system. In order to prove the capability of a fiber optic shape sensing system in a wind tunnel environment a flexible wing test article was constructed. The wing deflections and twists of the test article were modeled using a vortex lattice method called *Tornado* combined with simple beam theories. The beam theories were linear beam theories and the stiffness of the composite bodies was supplied by static testing of the test articles. The code was iterative in that it ran the *VLM* code to estimate the forces and moments on the wing and these were applied to a linear beam which gave the wing a new geometry which in turn was run through the VLM. The wind tunnel model was constructed at Virginia Tech using 3-D printing techniques for the fuselage and foam and fiberglass for the wings. On the bottom surface of the wings the Luna Technologies Inc. fiber optic shape sensing fiber was bonded along the leading and tailing edges. The swept-wing test article was experimentally tested in the Virginia Tech 6'x6' Stability Wind Tunnel at various airspeeds and the VLM based code results were in agreement, within margins of error and uncertainty, with the experimental results. The agreement of the analytical and experimental results verified the viability of using an iterative VLM code in combination with simple beam theories as a quick and relatively accurate approximation method for preliminary design and testing. The tests also showed that a fiber optic shape sensing system can be sufficiently tested in a wind tunnel environment, and if applied carefully could perhaps in the future provide useful shape and strain measurements.

Acknowledgements

I would like to thank my advisors, Dr. Schetz and Dr. Kapania for their constant advice and support with this project. Without their expertise and guidance this project would not have been accomplished. I would also like to thank Dr. Devenport for his assistance; and Mr. Evan Lally and everyone else at Luna Technologies for their collaboration, support and direction.

I would also like to personally thank my friends and family for their support and love. They made my time here much more enjoyable and fruitful. I would like to thank John Coggin for all of the help he gave me throughout the entirety of this project. Finally I would like to thank my fellow students for their support and encouragement: Eddie Hale, Mark Palfram, Maria Rye, Tom Kasmer, Matt Shepard, David Jingeleski, Dean Manno, Eric Faraci, Joshua Minnix, and Nik Patel.

Table of Contents

List of Figures

List of Tables

List of Equations

1 Introduction

In recent years there has been a surge in interest in the design of flexible wing aircraft. Unlike common aircraft wings long, slender, and flexible wings use far less material and therefore result in a significant reduction in structural weight.[14] In the 1980's Rockwell International Corporation began a project named the Active Flexible Wing concept. This project took advantage of the weight savings in a flexible wing in two ways, both with a low structure wing and no horizontal tail. These designs permitted large amounts of aeroelastic twist in order to provide improved maneuverability. In each of these concepts, multiple control surfaces are used to counteract the degraded roll performance that often results from flexible wings. A similar project, the NASA x-56 MUTT,[15] also hopes to take advantage of the structural weight savings of a flexible wing aircraft. A large concern of this project is the susceptibility to flutter, wind gusts, and atmospheric turbulence. Two key technologies NASA is working to advance are therefore gust alleviation and flutter control, both of which require information about the wing shape.

A shape sensing method that is gaining popularity is the use of fiber optic systems. Optical fiber sensors began as acoustic sensors in the late 1970's but since have proven to be useful for magnetic, pressure, temperature, displacement, and strain sensors since.[16] These sensors also have the added advantage that the fibers can be configured into any arbitrary shape. The system makes measurements using a laser beam that is sent through the fiber. The beam is sent through a reference fiber and then allowed to travel into the sensing section of the fiber. After travelling through the test section the signal of the sensing section beam is then compared to the reference using a photodetector and based on the organization of the light the difference

between the reference and the sensing state is analyzed and the desired measurement can be made. Fiber optics have also shown promise for medical applications.[17] Uncabled fibers are thin enough to be inserted directly into hypodermic needles and catheters minimizing the invasiveness of these sensing procedures. The sensors measure a variety of physiological parameters, such as body temperature, blood pressure, cranial pressure, and muscular strain to name a few. The versatility and relative simplicity of the fiber shape sensing system give it a wide range of uses and limitless possibilities in terms of application.

Luna Innovations has developed a fiber optic shape sensing system geared specifically for shape and strain measurement to address applications ranging from medical robotics to longer distance remotely operated vehicles (ROV's).[18] Their system uses optical frequency domain reflectometry (OFDR) to obtain high density strain measurements from multiple cored optical fibers. The measurements are made by extracting the light signal reflected back from either continuously written Fiber Bragg Gratings (FBG's) or from the Rayleigh scatter signature of the optical fiber itself.

The design and modeling of the flexible wing aircraft was a problem in computational aeroelasticity (CAE). Aeroelasticity is the investigation of the interaction between fluid dynamics, structural dynamics and structural elasticity. The understanding of the interplay between these three is the key to the real time wing shape and therefore is essential to problems of flutter, gust response, and flexibility-induced effects on stability and control. For much of the history of flight, people interested in aeroelastics have relied on wind tunnel and flight testing supplemented with empirical and theoretical methods.[19] The advent of digital computers has given aeroelasticians the capabilities for computational fluid dynamics (CFD) and computational structural dynamics (CSD), the combination of the two has being CAE. In terms of using these

computational methods to model lifting surfaces such as wings there have been many successful research efforts and commercial codes written specifically with the goal of aeroelastic prediction in mind; namely ENSOLV, EURANUS, and AETHER to name a few.

In this study the focus is to model the aeroelastic behavior of high aspect ratio wings in low subsonic flow fields. Due to the high flexibility of these wings the coupling of aerodynamics and structure is an important design issue. Many efforts in this area have focused on the responses in non-steady state conditions and dynamic instabilities of the wings, such as flutter, because this is where the greatest issues in aeroelasticity lie. Eskandari and Dardel focused their efforts on the modeling of a thin wing immersed in a quasi-steady flow field.[20] The aerodynamics, such as the lift and moment distribution along the wing, of their case was modeled according to quasi-steady aerodynamic theory while the coupled structural model was a second order ODE which served as an equation of motion for the wing. The goal was to understand the behavior of long and slender wing-like surfaces, one example was helicopter blades, at very high airspeeds. A similar study done by Stragnac and Mook used an unsteady vortex lattice method (UVLM) to model the aerodynamic loads and a coupled structural comprised differential equations of motion for a cantilever wing. [21] This effort was focused on the transient response of the wing exposed to the unsteady flow field.

Although much aeroelastic work has focused on dynamic instabilities there has also been much work done on wing response due to steady aerodynamic loads. This field has primarily been interested in flexible high aspect ratio wings for high altitude flight because of their beneficial flight endurance characteristics. One such study performed by Bond and Canfield et al, studied the joints of a flexible wing aircraft with a bracing system of multiple wings which was dubbed a joined wing.[22] These joints were modeled using an finite element method (FEM)

which was subjected to expected aerodynamic loads based on experimental data. A test article was also constructed in order to validate the FEM and the results were compared to experimental results measured using strain gauges placed around the joint. Another study performed by Zhang et al studied the control of flexible high aspect ratio wing response to aerodynamic forces which were experimentally derived.[23] Again the structure was modeled using a simple FEM. The results of this study provided the theoretical differences between the rigid and elastic properties of a wing such as changes in effective angle of attack, the forces that the wing is subject to as well as expected tip deflection and twist angles at a few angles of attack.

There has also been work done with the goal of predicting the response of wind tunnel models using a combination of simple CAE methods. The Smart Wing Project was a forward thinking project in which the goal was to demonstrate that smart materials, such as shape memory alloys, could be used to increase aerodynamic performance of a wing by varying the wing geometry during flight to better match real time flight conditions.[24] In 2004, Martin et al, constructed a test article to test the smart material control surfaces in a wind tunnel environment. The wind tunnel model featured 10 individual smart material trailing edge segments, embedded in the wing structure, which would be able to deflect and effectively change the wing geometry at one second intervals. For this project there was also a theoretical model which informed the design of the test article and was compared to the experimental results. The aerodynamic loads were calculated by a doublet lattice method and then an FEM predicted the expected wing deflections given the wing geometry. A similar, but slightly simpler, study was performed on a high aspect ratio wing of a BWB aircraft by Carlsson in 2005.[25] The study focused on the performance characteristics of the wing and control surface due to the change in geometry caused by the actuation of a control surface. This wing was a fiber carbon and epoxy composite,

the aerodynamics of the wing was calculated with a doublet lattice method and these loads were coupled to the structure of the wing using NASTRAN. In each of these cases the wings are deflecting due to control surfaces and not the base wing loads. For this study the wing is so flexible that even small aerodynamic loads can cause a significant change in wing geometry.

The aim of this study was to design a flexible wing test article that would demonstrate the capability of the Luna Innovations shape sensing system specifically for aerospace applications. In order to accomplish this task a flexible wing test article was designed, modeled, and experimentally tested in both open and closed section wind tunnels. The wing was modeled using linear beam theory and the aerodynamic loads were calculated using a vortex lattice method. The test article itself was to be a swept wing with high flexibility and low natural frequencies, much like the NASA x-56 MUTT. The fiber optic shape sensing system was to be attached and the reference section would be housed safely in the fuselage. The shape sensing system would give rapid wing deflection and twist measurements under the load of a steady wind tunnel flow. Crude experiments would be carried out in the open jet wind tunnel in order to check the functionality of the system and then more precise experiments were to be carried out in the Virginia Tech Stability Wind Tunnel.

2 Modeling Methods

2.1 Aerodynamic Loads

Tornado is a vortex lattice method that is run in MATLAB.[4] Like many vortex lattice methods, creates a flow field that assumes incompressible, irrotational, and flow.[1] For this study the assumption of incompressible flow is acceptable because the wing being analyzed will be tested at speeds where compressibility effects are negligible.[12] This flow filed also assumes that

the line integral between any two points, independent of the path, is zero; as such this is a conservative flow field. In the case of fluid flow a velocity potential is defined so that $\vec{V} = \nabla\phi$, where ϕ is the potential, this same equation satisfies the condition of irrotationality because it implies that the curl of the velocity is zero. It also imposes that no mass is produced within a given flow field so that $\nabla \cdot \vec{V} = 0$. Complex irrotational, incompressible flow pattern can be synthesized by adding together of elementary flows which are also incompressible and irrotational, in the case of the vortex lattice method the flow field is created by adding several line vortices.

Line vortices induce a flow field around the line with the flow direction perpendicular to the radius from the line and the strength inversely proportional to the magnitude of the radius. In *Tornado* these line vortices are of finite length, also called vortex segments. The induced velocity for a vortex segment of infinitesimal length is given by the Biot-Savart law and is shown in equation (1).

$$d\vec{V} = \frac{\Gamma\left(d\vec{l}\times\vec{r}\right)}{4\pi r^2} \qquad (1)$$

In equation (1) *r* is the distance from the segment to the point of interest, *dl* is the infinitesimal length of the segment and Γ is the strength of the vortex. This equation can be integrated along the length of a vortex segment to give the induced velocity field of the entire segment.

Tornado deals with lifting surfaces such as wings, fins and canards. For the case of this study it will be used for the analysis of flexible wings. These surfaces are broken up into panels, the number of which can be defined by the user, and on each of these panels vortex segments are

placed in a horseshoe pattern as shown in Figure 2.1. The flow field from all of the vortices creates a downwash on the panel; the velocity of this downwash is accounted for by enforcing a boundary condition that prevents flow through the panel. This boundary condition is enforced at the collocation point of the panel, marked by the little "x" in Figure 2.1. Using this boundary condition the strength of each vortex is calculated. After this is done the free stream flow is added to the flow field at the lifting vortex, the top of the horseshoe, mid-point. The induced velocity from this condition may be used to get the force acting on the panel by the Kutta-Jukovski theorem, shown as equation (2). In this equation F is the force on the panel ρ is the density and all other values are as previously defined.

$$\vec{F} = \rho(\vec{V} \times \vec{\Gamma}) \cdot l \qquad (2)$$

In this study, the structural model will be discussed later in this document; the forces of influence are those that create bending moments on the wing. *Tornado* calculates the bending moment on the wing by breaking the wing into chordwise strips at each station along the span. The net moment on those strips are calculated by summing the forces on each chordwise panel in a given strip and then multiplying that by the distance to the origin of the coordinate system. This gives the net moment on the strip and when done on each strip along the span the distributed bending moment of the wing is calculated.

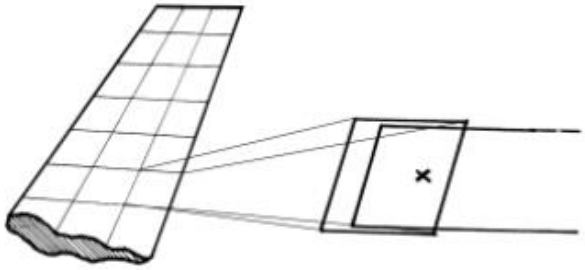

Figure 2.1: Example of panel arrangement and horseshoe vortex placement for *Tornado*

The construction of the lattice begins with a user defined geometry and number of panels. The horseshoe vortices are placed using the coordinates of the corners of each panel. In *Tornado* the top of the horseshoe is placed on the quarter chord of the panel and spans the length of the panel. The collocation point of the panel, which is where the downwash boundary condition is applied, is in the middle of the panel at three quarters of the panel chord. Unlike traditional vortex lattice methods, which use only three vortex segments to create the horseshoe, *Tornado* uses seven. The horseshoe begins at 15 times the distance between the collocation point and the vortex segment, or half of the panel width, behind the trailing edge of the panel. To be mathematically correct the trailing wake should extend to infinity, for the sake of real numerical methods the length of the trailing vortex segments is truncated. The influence of the segment as the length increases on the downwash boundary condition is shown in Figure 2.2. This distance of 15 times the distance between the collocation point and the vortex line is chosen because at this distance the added influence is essentially zero.

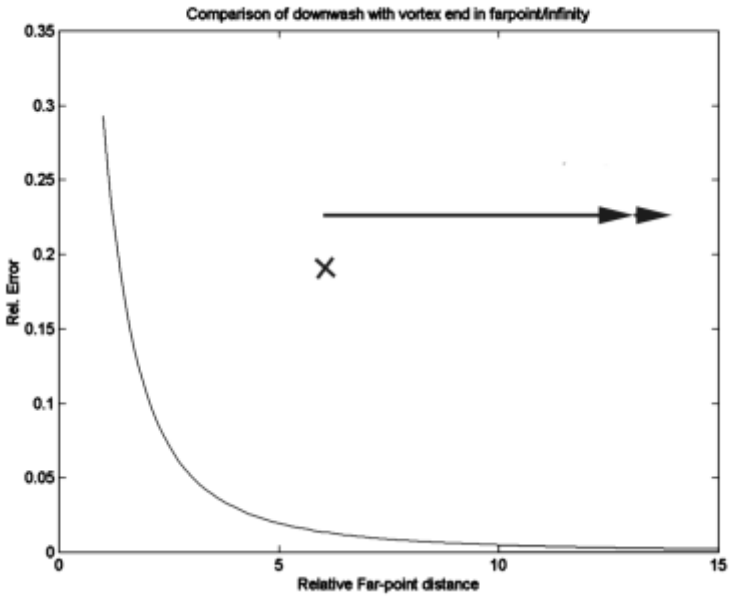

Figure 2.2: Relative error as length of vortex segment increases

The second vortex segment begins at the trailing edge of the wing, the third at the hinge line of the control surface if there is one. The fourth vortex segment is the segment that goes across the panel at the quarter chord, the top of the horseshoe. The other three segments travel down the other side of the panel in the same fashion as the first three. It should be noted that unlike many vortex lattice methods which allow the trailing vortices to go straight out from the wing, the vortex segments in *Tornado* realign with the free stream.

The vortex lattice method was compared to test cases in order to validate the functionality of *Tornado*. For comparison the author references an example from a text which compares a vortex lattice method to experimentally measured values of the lift of a wing with known geometry.[3] The results are shown in Figure 2.3.

The data and the *Tornado* results match very well especially at lower angles of attack. The differences at higher angles of attack are likely due to thickness effects. *Tornado* assumes

that the airfoil is a line, and as such, does not account for airfoil thickness. It does this by placing the panels along the chord line. For cambered airfoils the only change is that the boundary condition is applied in the direction of the camber line, the location of the panels does not change. A visual representation of this is shown in Figure 2.3.

Figure 2.3: Sample panel layout for cambered airfoil

Tornado has also been compared to commercial vortex lattice codes to great effect. For more detail please see the MS thesis of Thomas Melin.

A significant advantage of low level CFD methods such as the *Tornado* is the small amount of computing time. This code simply runs the geometry once and treats it as a rigid body; from this, the coefficient of pressure can be inferred on each panel and by summing the forces on the panels the net aerodynamic forces and moments on the wing can be calculated. The first problem is that in the real world and especially in this study the wing is not rigid, another problem is that these codes are not naturally iterative in geometry. To combat this issue it is possible to modify the geometry after each step according to the incident forces on the lattice, change the geometry accordingly, and then run the software on the new geometry. Due to the low level of computing required in the VLM solutions, iterating the geometry to a state of geometric convergence is not out of the question even for a relatively low-power processor.

The geometry and state inputs are accepted as structure arrays. The structure arrays or *structs* may contain several vectors in different indices, allowing many inputs to be contained and transferred between sub-functions easily. As an example, the structure array inputs for the geometry of the swept wing model, as well as a sample state structure, are given in the appendices.

From the state and geometry structure arrays *Tornado* uses sub function *fLattice_setup2* to create the vortex lattice. The vortex lattice is a planar lattice that simulates a three-dimensional wing using thin airfoil theory by insuring that there is no flow through the camber line. The vortex strength in different areas of the lattice is varied in order to meet this criterion. A sample output of the swept wing model lattice and pressure distribution is shown below, in Figure 2.5. The color of each panel is dependent on the pressure on the panel, the deeper the shade the stronger the pressure.

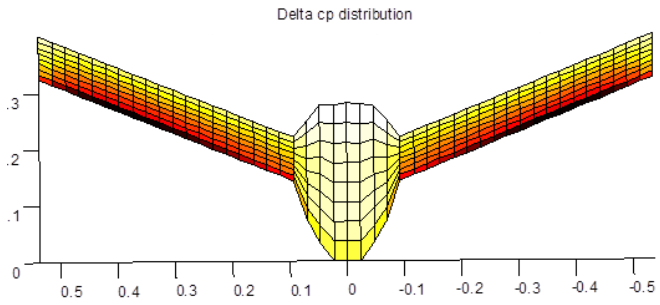

Figure 2.4: Typical Pressure distribution on swept wing model from Tornado

The lattice is then used to calculate forces on the wing based on the pressure distribution induced by the free stream and vortex lattice using sub-function *solverloop5*. The solver function

is capable of producing several results based on the lattice including parameter sweeps, time derivatives of angular accelerations, and viscous drag estimations to name a few. For this work, a static calculation at the selected state was run. The output from the solver sub-function includes the bending moment along the span as well as the moment on each of the panels in the lattice.

2.2 Bending and Twisting

2.2.1 Stiffness Modeling

Due to the fact that the wings are made of different materials, foam, epoxy and glass, the stiffness properties must be calculated as an equivalent beam. The stiffness properties of the composite wing constructed of foam, fiber glass, and fiber layup were first approximated by a method of equivalent areas.[5] The idea is that a section composed of one or more materials can be defined as a section of a different shape made entirely of only one of the materials in the section. The resistance to bending of the bar would remain the same if all portions were made of the same material provided that the width of the sections composed of other materials were multiplied by a factor *n.* It is important to note that the width must be taken in the direction parallel to the neutral axis. Here the factor *n* is a ratio of the Young's modulus of the materials $n=(E_i/E_b)$ where E_i is the Young's modulus of each other portion to be multiplied by *n* and E_b is the modulus of the reference material.

The aforementioned model was used to predict the stiffness of early iterations of the constructed composite wings. The first wings were NACA 2410 airfoil shapes of expanded polystyrene (EPS) foam with a 2 inch chord, and the fiberglass skin was 0.001 inches thick. The method of equal areas when applied to the composite wing predicted a bending stiffness of 17.6 lb-in^2. The actual stiffness was measured experimentally by hanging weights from the tip of the

wing and measuring the deflection. The empirical data from tip deflection experiments yielded a stiffness of 18.4 lb-in^2. This approximation worked well for earlier iterations but was inadequate for later iterations due to scaling issues.

The stiffness of the constructed composite wing was also very dependent on the amount of epoxy used to bond the fiberglass to the foam core. In the earlier iterations, very thin fiberglass was bonded using a minimum amount of epoxy. As the construction process was refined and the stiffness required to withstand the aerodynamic loads increased, however both the amount of epoxy used to bond the fiberglass, and the thickness of the fiberglass layer itself, were both increased. The airfoil shape remained an NACA 2410, but the chord was increased to 3 inches and the fiberglass thickness increased to 1.5 ounces per square yard. Although this change appears small, it greatly affected the amount of epoxy necessary to bond the fiberglass skin to the foam core.

The torsional stiffness of the section was originally modeled by an elliptical cross section, but after iteration the ellipse was found to be a poor approximation. Currently the torsional stiffness is calculated through empirical data and then fed directly into the twist calculation. The torsional stiffness was determined by placing a weight off center on the tip of the wing and then measuring the angular rotation. Using the information of the length of the wing the following equation was used to calculate torsional stiffness.[6]

$$\phi = \frac{TL}{GJ} \qquad (3)$$

Where T is the applied torque, the length is represented by L, GJ is the torsional stiffness, and ϕ is angle of twist. The torque on the wing was calculated by *Tornado* and a differential form of eq. (1) was used to calculate the wing twist.

As previously mentioned, the theoretical modeling of the stiffness properties became less accurate as the model became more complex. Because of this, the properties were found through experimental measurement and then these numbers were used in the analytical bending and twisting calculations. The shear center of the airfoil was also estimated through static testing as numerical methods proved unsuccessful. An outline and the results of these experiments are given in the appendices.

2.2.2 Bending

The bending moment along the span calculated by the *Tornado* solver sub function was used in combination with the measured bending stiffness to predict the deflection of the wing under the specified aerodynamic loads. The deflection calculation was handled using Euler-Bernoulli beam theory, more specifically the equation below. Euler-Bernoulli beam theory is a simplification of the linear theory of elasticity that assumes the beam is a line called the neutral axis. [7] The neutral axis deflection can then be calculated by integrating the bending moment applied as shown in equation 2. This approximation, while invalid for thick and short beams, is adequate for longer beams such as high aspect ratio wings.

$$w(x) = \int_0^x \int_0^\eta \frac{M(\xi)}{EI} d\xi d\eta \qquad (4)$$

In eq 2, *M* is the bending moment along the span, *w* is the deflection, and *EI* is the stiffness of the section which is undergoing bending. For the NACA 2410 section the shear center, experimentally calculated to be at 37 % chord, is used as the elastic axis. It is also worth noting that this theory, because it is linear, is sufficient to model bending in both swept and non-swept wings without altering the boundary conditions. For swept wings a modification to twist modeling must be made.

2.2.3 Twisting

In addition to providing the bending moment in the wing, *Tornado* also calculates the twisting moment on each panel in the lattice. This torque was applied along an axis running through the shear center of the airfoil shape, called the elastic axis, and in combination with the measured torsional stiffness the wing twist was calculated using eq 1. In the unswept wing case, which was studied first, the twisting calculation was carried out using only the torque about the elastic axis, but the swept wing case was more complex because the observed twist due to bending must also be accounted for.

The first step was to use a coordinate transformation in the form of a rotation by the angle of sweep around the yaw axis in order to transform the moments onto the wing. In this transformation the moment vector *M*, which contains the moments on each panel, becomes *M'* through equation 3 shown below. In eq. 3, both *M* and *M'* are 3xn vectors containing the moments of *n* panels on all three axes, and θ is the angle of rotation.

$$[M'] = \begin{bmatrix} \cos(\theta) & \sin(\theta) & 0 \\ -\sin(\theta) & \cos(\theta) & 0 \\ 0 & 0 & 1 \end{bmatrix} [M] \qquad (5)$$

The new *M'* vector then contains the moments on each panel with respect to the new rotated axes. The only axis of interest, however, is the axis that runs along the wing on which the twist acts directly.

The second correction for a swept wing is the coupling between bending and twisting of the wing. *Tornado* defines the lattice as perpendicular to the free stream, and as such the panel definition and the axis of bending are not perpendicular in the case of a swept wing. As shown in

Figure 2.5 the panels of the lattice are not rectangular, and because the panels are defined inboard, the angle of the wing due to deflection at each station contributes to the twist angle of each panel as shown in equation 4.

$$TWn = \arctan[\cos(sw) * \tan(TWi) - \sin(sw) * \sin(dw)] \quad (6)$$

The above equation transforms the twist *TWi*, which is calculated using equation 1, into the frame of the inboard panel lines by taking into account the sweep angle *sw*, and the angle of each station due to deflection *dw*. The twist is positive counterclockwise.

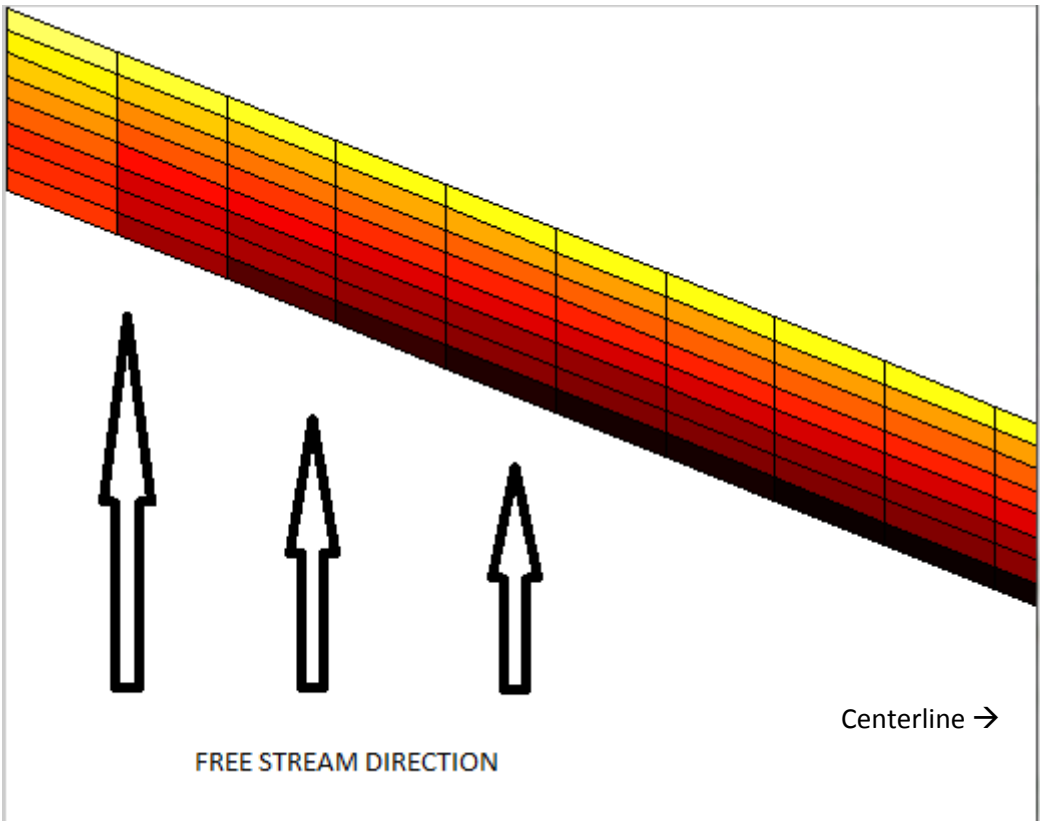

Figure 2.5: Swept wing panel layout

With the twist and bending along the wing properly modeled, *Tornado* could be automated and iterated in order to properly model the way that the aerodynamic loads change because of the wing shape and eventually converge on a stable equilibrium.

2.3 Iteration

In order to ensure that deflection and twist were being modeled as closely to the test conditions as possible, the geometry of the lattice needed to be changed with the deflections and twists calculated in the wing. With the change in shape, the aerodynamic loads on the wing change and deflections are then recalculated, and this process is repeated until the deflection converges. Figure 2.6 shows iterated lift loads to convergence for the swept wing model at 96 ft/s and 4 degrees angle of attack. The dimensions of the swept wing theoretical model are given in Table 2.1.

Table 2.1: Geometry of swept wing model in *Tornado*

Airfoil Shape	NACA 2410
Chord Length	3 inches
Wing Span	42 inches
Wing Sweep	22 degrees
Taper Ratio	1

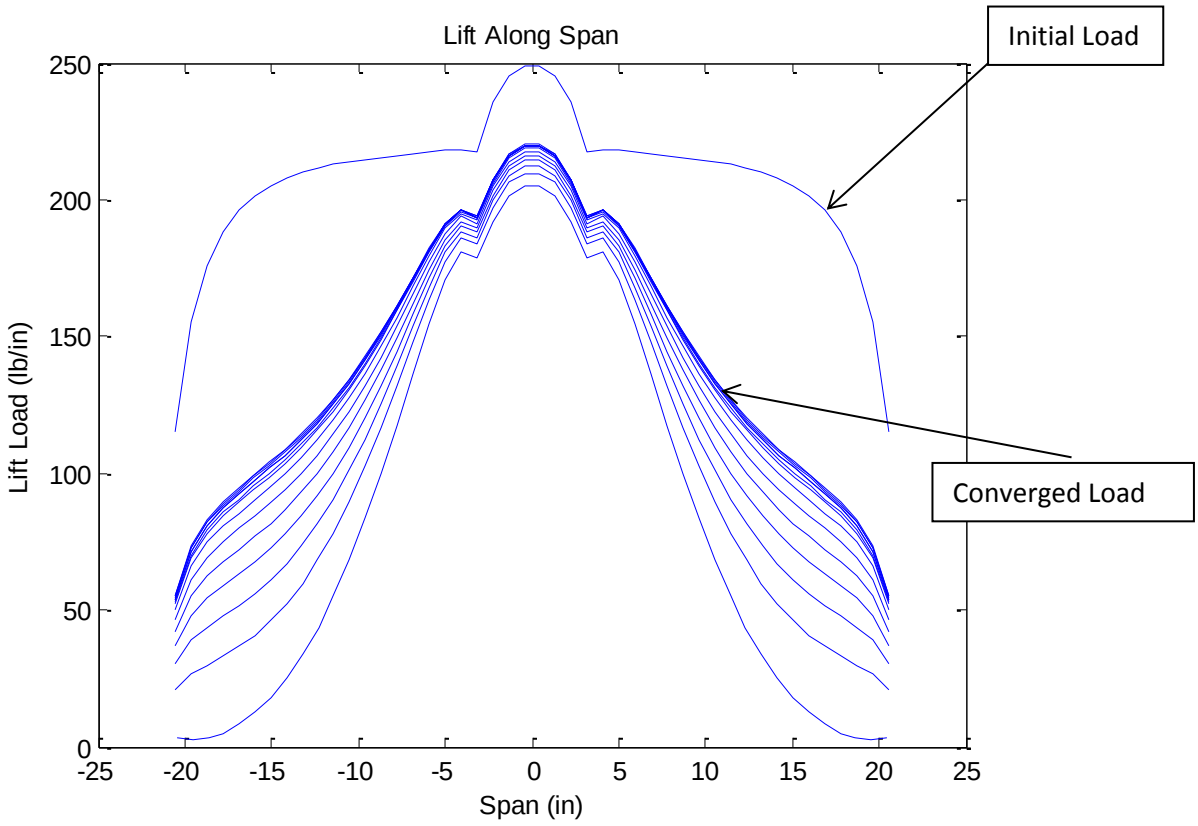

Figure 2.6: Iterated lift load along span, each individual line corresponds to unique geometry

The geometry struct array was iterated using a while loop and a convergence criterion of 0.05 % tip deflection change by span, which equated to about 0.007 inches; meaning that if the wing tip deflection did not change by at least 0.007 inches from the previous iteration the calculation would be considered converged. After convergence the iterated geometry is plotted as shown below in Fig. 2.7 at the same conditions as used for obtaining results shown in Fig. 2.6.

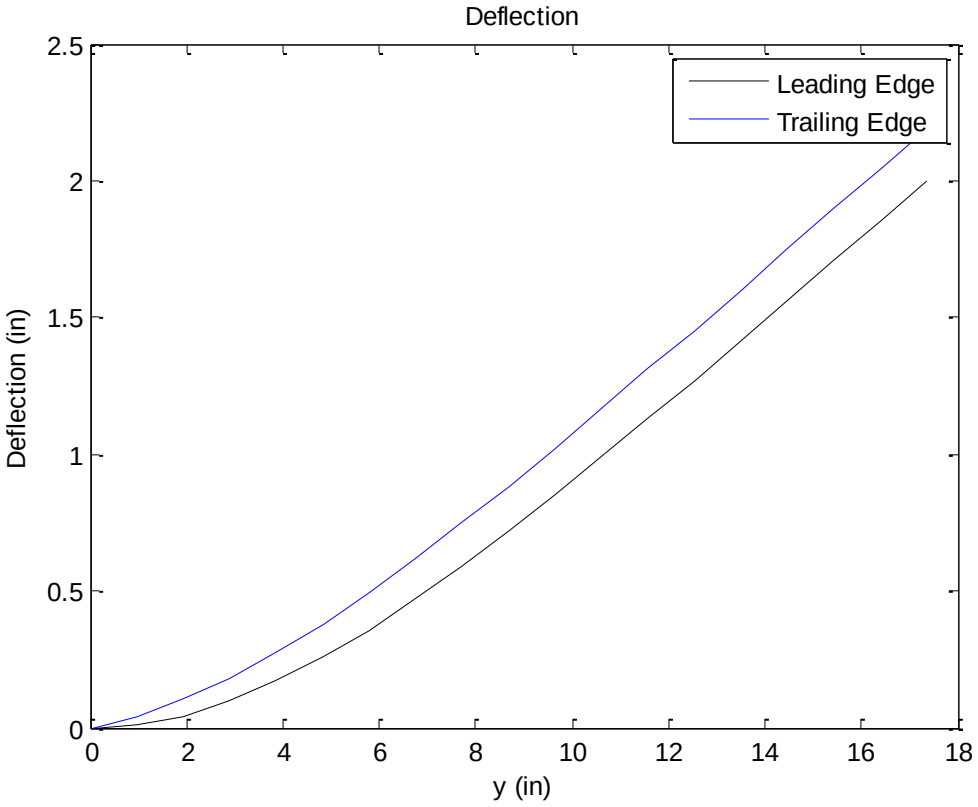

Figure 2.7: Final deflection after iteration for the swept wing model

The final deflection shown above is the data that is to be compared to the results from wind tunnel testing. The number of panels used in the numerical investigation was determined in order to balance the time of the calculation with the precision of the measurement. The grid size was varied as shown in Table 2.2 in order to demonstrate the grid independence of the calculation. The grid size is the number of panels on each wing, the number of chordwise panels was varied in order to change the grid size. The number of spanwise stations was not varied due to significant increase in computational time with no change in results.

Table 2.2: Change in tip deflection due to change in grid size

Grid Size	% change in tip deflection
160	0
180	0.1519757
200	0.2279635
250	0.2279635

Tip deflection was chosen as the grounds for comparison because it is the point of calculation which would suffer the most change due to a load change. As the grid size is increased the time of calculation increased steeply; as such the lowest grid size of 160, which equates to 8 chordwise panels and 20 spanwise panels, was chosen for the numerical model.

3 Model Construction and Measurement Methods

3.1 Unswept Wing

The unswept wing test article was designed and tested in order to gain rudimentary knowledge on how a wing with a fiber bonded to the surface would perform in a wind tunnel environment. It was constructed and tested rapidly so that efforts towards the completion of the full-span model could be focused. As such only open-jet wind tunnel tests were performed and the construction was minimal. The wing was a 2 inch chord expanded polystyrene (EPS) foam core wing in the NACA 2410 airfoil shape. On the bottom of the airfoil a dummy fiber was also bonded using a simple five minute epoxy as shown in Figure 3.1. The wing was then skinned with a thin sheet of fiberglass. The details of the dimensions of the unswept wing are given in Table 3.1.

Table 3.1: Details of construction for unswept wing experimental model

Airfoil Shape	NACA 2010
Chord Length	2 inches
Length	14 inches
Fiberglass Thickness	0.5 oz/yd^2

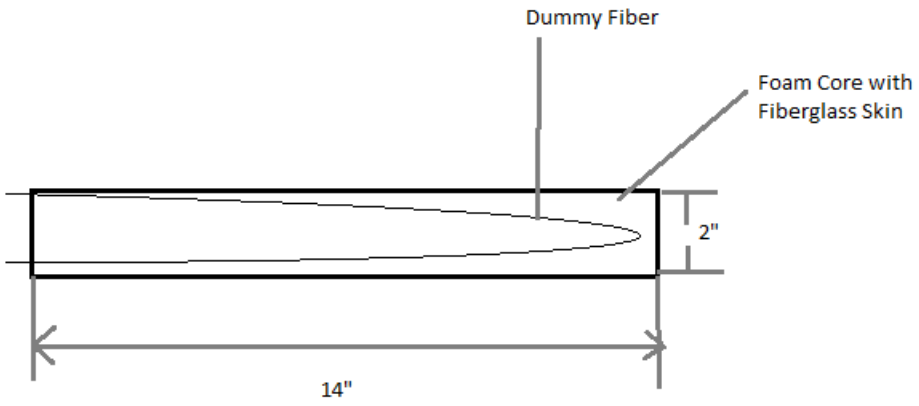

Figure 3.1: Drawing of fiber layout on unswept wing

3.2 Swept Wing Full-Span Model

The full-span test article was designed to be a small scaled version of the NASA x-56 type aircraft. The fuselage was made using Objet 30 3-D printers supplied by the VT Machine Shop. This machine provided a relatively smooth hard plastic fuselage piece with inner and outer sections, as shown in Figure 3.2. These clamshells were designed to accommodate the airfoil shape of the wing. The fuselage was also designed to fit to an already existing strut mount that had seen previous stability tunnel testing. In order to ensure angle of attack, a 2 degree angle of

attack as built into the fuselage model. The design CAD drawing of the assembly is shown below and the completed pieces are shown below that. The printed results of the clamshell are shown in Figure 3.3.

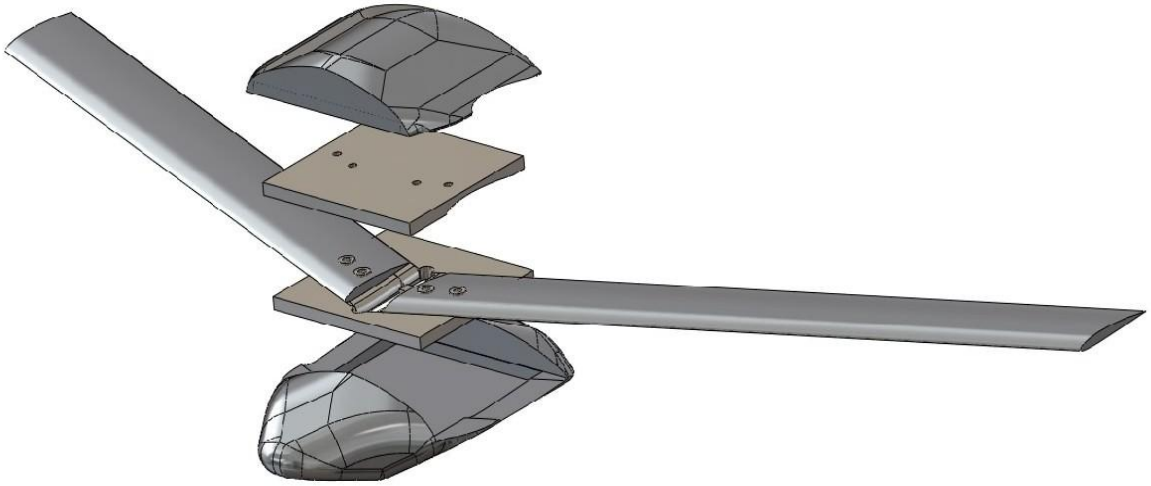

Figure 3.2: CAD drawing of assembly

Figure 3.3: Inner and outer clamshell fuselage pieces (outer on right; inner on left)

The wings were a foam and fiberglass composite. The EPS foam cores were purchased from flyingfoam.com, were a NACA 2410 airfoil section, and had a 3 inch chord. The fiberglass

density was 1.5 ounces per square yard and was bonded to the wing using common 60 minute epoxy. The wings were designed to fit into the model with a 22 degree sweep and were cut down to fit as shown in Fig. 3.4.

Figure 3.4: Photograph of completed wings

The holes in the wings were put in place so the inner clamshell of the fuselage mold would hold the wings in place within the fuselage. The clamshell pieces also accommodated Luna Technologies fiber optic shape sensing system. The fibers began in the center of the model, running up the spar and into the bottom of the fuselage and then ran along the wing from root to tip and back on both wings. The fibers were bonded to the wings using a silicone based epoxy so as not to add too much stiffness to the wing. Figure 3.5 shows the fiber routing pattern on the bottom wing. Table 3.2 shows the detailed geometry of the swept wing model.

Table 3.2: Details of construction for swept-wing model

Airfoil Shape	NACA 2410
Wing Sweep	22 degrees
Taper Ratio	1
Angle of Attack	2 degrees
Chord Length	3 in.
Wing Span	42 in.
Fiberglass Thickness	1.5 oz/yd^2

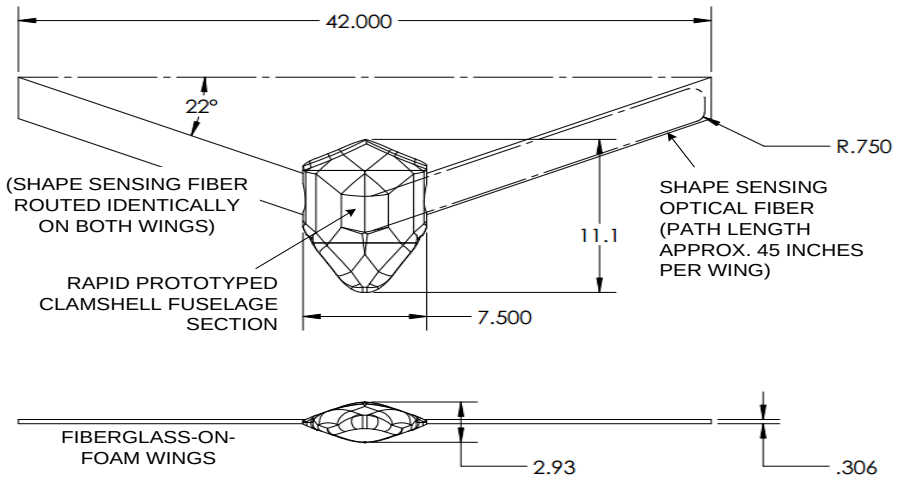

Figure 3.5: Drawing of test article showing fiber routing pattern all measurements in inches

The strut was composed of a single rectangular beam covered by 3-D printed airfoil shaped plastic filets. A photograph of the strut is shown in figure 3.6.

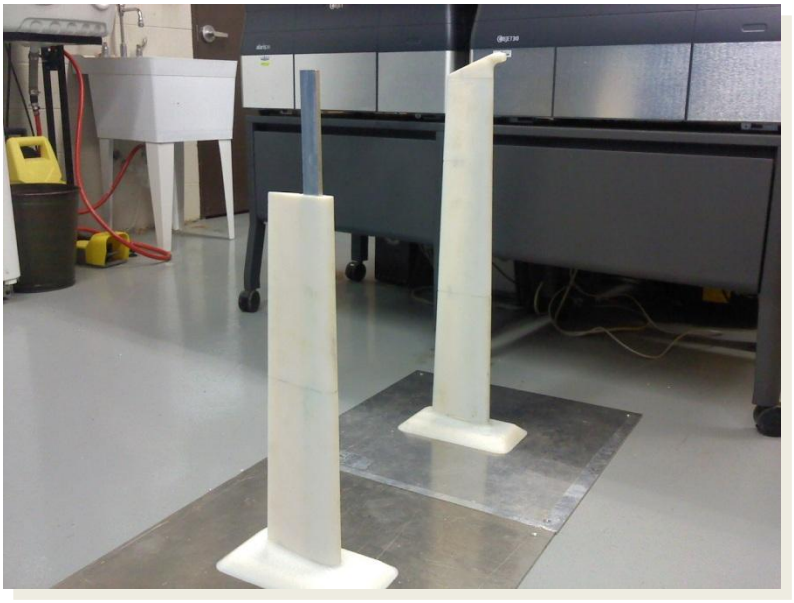

Figure 3.6: Strut on which test article was mounted. (front of picture)

The strut was braced on either side by cables attached to an airfoil shaped aluminum filet which was then bolted to the base plate of the strut; this guarded the filets from stress due to lateral movement. The top of the rectangular beam rested within the model and was fixed to the fuselage by two small screws. The setup of the strut, plate, and model, as well as the experimental setup of the swept wing model are discussed further in Chapter 4.2.

3.3 Measurement Methods and Uncertainty

Experimental measurements were made in only one way in the open-jet tunnel experiments, but in two ways in the Virginia Tech Stability Wind Tunnel experiment. In the open-jet test a ruler was used measure the deflection of the leading and trailing edges of the wing tip relative to a reference point measured while there was no flow through the test section, the smallest grid size on this ruler was $1/16^{th}$ of an inch bringing the measured uncertainty to

0.03125in. The experiments performed in the Virginia Tech Stability tunnel did not use a ruler and instead used a photographic grid method, and a laser distance measurement.

On the outside of the wind tunnel, a Nikon D7000 camera was mounted on a rail and used to take pictures of the wing tip. Using this photograph set up, a gridded piece of paper was also photographed. By using Microsoft PowerPoint the grid image was overlayed on the wing image. Using the zero deflection image as a reference, deflection and twist measurements were made. The images in Figs 3.7 and 3.8 are shown as examples. Each grid square is equitable to 0.2 inches and it can be read to within 0.25 grid squares of accuracy so the uncertainty in these measurements was 0.05 inches, in order to reduce this future studies could include finer grid meshes.

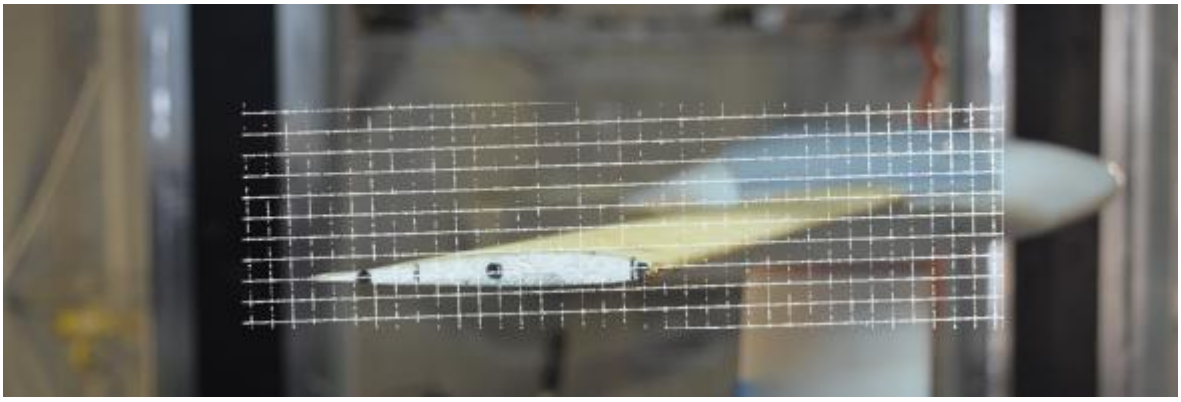

Figure 3.7: Photograph with grid overlay of undeflected geometry

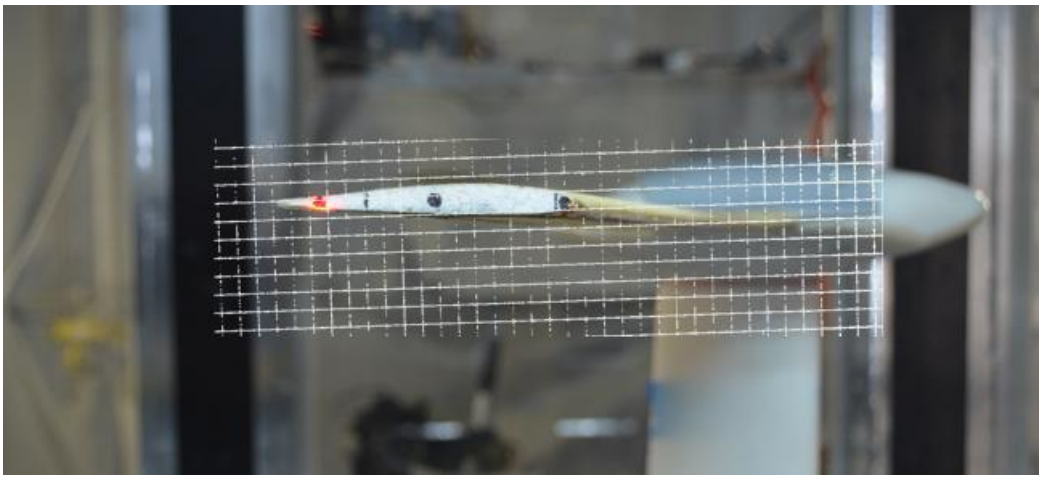

Figure 3.8: Photograph of grid overlay with deflected geometry

The second form of measurement in the 6'x6' tunnel experiment was made by a laser distance measurement device. This device was pointed at the wing through a transparent plate on the floor of the wind tunnel and measurements of leading and trailing edge positions were taken at each airspeed and then compared with a reference. The uncertainty on the device was 0.05 inches. It is likely that the error in the measurement was slightly greater because it also depended on the location at which the laser was focused on the wing. The laser was held by human hands and pointed at the wing manually and this adds further uncertainty to the laser measurement.

A third form of shape measurement being utilized in the experiment was performed by Luna Technologies. A fiber optic cable bonded to the bottom surface of the wing ran through the fuselage section and was run through the bottom of the tunnel and attached to Luna data acquisition hardware. Unfortunately none of this data was useful and as such is not included in this work.

4 Results

4.1 Unswept Wing Model Results

Experimental testing of the unswept model was done only in the Virginia Tech open throat wind tunnel [8]. A photograph of the wind tunnel is shown in Fig 4.1.

Figure 4.1: Virginia Tech Subsonic Open Jet Wind Tunnel

The tunnel is a blower type and the fan discharged into a 6 degree, 13.1' long diffuser. The flow then passes through a 57.9 x 70.1" wide settling chamber followed by a combination of 0.4" meter cell size, 3.6" long honeycomb and three turbulence reduction screens made of fiberglass with a 55% open area ratio. The flow velocity is measured using static pressure taps located at the exit of the settling chamber. At the highest fan speed the flow exits the 5.5:1 contraction at 96 fps. The open throat tunnel had a 27 3/8" square test section outlet and the unswept wing was mounted in the test section as shown in Fig 4.2. After passing though the test section the flow is stopped by a jet backstop located 3.9' downstream from the contraction exit.

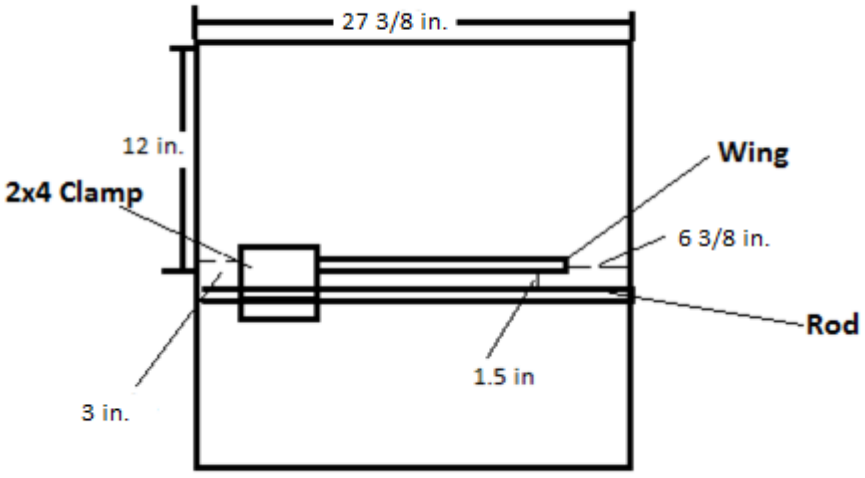

Figure 4.2: Drawing of unswept wing test set up, flow direction out of the page

The wing was clamped in a foam bed to 2x4 blocks which were in turn attached to a rod running span wise through the test section. The angle of this rod could be actuated and thus the test could be run at several angles of attack. The angle of attack was measured with an inclinometer which could be read with confidence within 0.5 degrees. A photograph of the setup is shown in Figure 4.3.

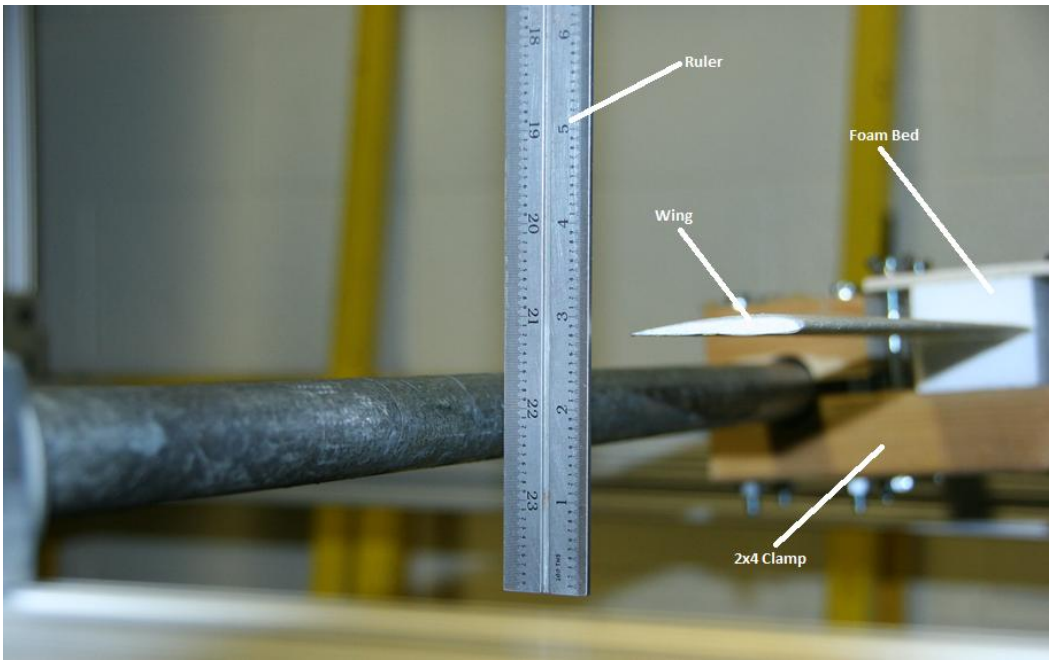

Figure 4.3: Open jet unswept wing experimental setup

Tip deflection and twist measurements were made with the ruler. It should be noted that the twisting moment on the wing was small enough that the twist of the wing was negligible. The theoretical model assumes that the wing is exposed to true free stream flow. In a wind tunnel environment the boundary conditions are different than in actual flight and these differences must be accounted for. In the open jet wind tunnel environment the corrections for streamline curvature and downwash effects are the most important to this study as they change the effective angle of attack of the wing.[9] The effective change in angle of attack follows from equation (7).

$$\alpha = \alpha_u + \delta \frac{S}{C} C_l(57.3) \qquad (7)$$

In this equation δ is a constant based on the shape of the test section, *S* is the wing area and *C* is the cross sectional area of the wind tunnel. Applying equation (7) the effective angle of attack change for the wing due to streamline curvature is roughly -3% of the set angle of attack

of the wing. In addition to the downwash corrections the open jet wind tunnel also has an issue with the jet shear boundaries. On the edge of the exposed flow the atmosphere and the jet interact and a turbulent layer is formed around the laminar jet. This area grows as the flow continues downstream by an estimated 0.2 times the distance from the wing tunnel exit. The unswept wing test article was about 14 inches from the mouth of the wind tunnel which suggests that the turbulent layer was about 3 inches thick on either side of the test section meaning that the unswept wing should have been outside the jet shear layer.

As shown in the set up the unswept wing was also near a block and cylinder. In order to investigate the effects of these disturbances to the flow field and how they affected the wing the cylinder and block were modeled as elementary flows. In order to model the cylinder's effect the wing and cylinder were treated as a two dimensional flow and the streamlines of the flow were analyzed with and without the cylinder, 2" aft of the trailing edge of the wing, in the flow. From this it was estimated that the effective angle of attack of the model was lowered by 15 % by the rod as well as the effective airspeed decreased by nearly 4 %. The block, a blunt body, was modeled by a point source in three dimensions and the strength of this source was approximated using the dimensions of the 2"x4" block. The primary effect on the flow field the block had was displacement of the flow around the surface of the block and thus the slowing of the effective airspeed around the wing. This effect decreased with distance from the block. The effective flow speed at the root of the wing is estimated to have lowered by 8 % due to the block while the flow at the tip decreased by less than 0.5%.

The experiment was run at three airspeeds for each angle of attack, and then the results were compared to the theoretical model predictions. A tabulated comparison is given below.

Table 4.1: Open jet test results for unswept wing

	Deflection (in)							
Airspeed (fps)	**0 deg Exp**	**0 deg Theory**	**2 deg Exp**	**2 deg Theory**	**4 deg Exp**	**4 deg Theory**	**6 deg Exp**	**6 deg Theory**
14	0.05	0.09	0.9	0.18	0.15	0.26	0.3	0.35
20	0.15	0.21	0.26	0.4	0.4	0.6	0.75	0.79
26	0.3	0.37	0.71	0.72	1.1	1.08	1.46	1.40

Although there were several sources of uncertainty the measured and theoretical results matched well. Measurements were difficult to make because the wing oscillated, especially at lower angles of attack. As expected, due to the wind tunnel effects as well as the interference of the rod and block the measured results were consistently lower than the theoretical calculations. Despite the uncertainty and the oscillation the success of a flexible wing test article, with a fiber bonded to the surface, in a wind tunnel environment merited further testing.

4.2 Swept Wing Model Results

The first stage of testing of the full-span model was to perform preliminary experimentation in the smaller and more available open-jet wind tunnel in order to confirm the functionality of the optical fiber. Although due to the size of the test article the entire span could not be placed in the flow and testing was run on the half span. It was fixed in the tunnel by attaching the plate on the bottom of the strut to two horizontal beams that were bolted to the wind tunnel frame. A drawing of the setup is shown in Figure 4.3.

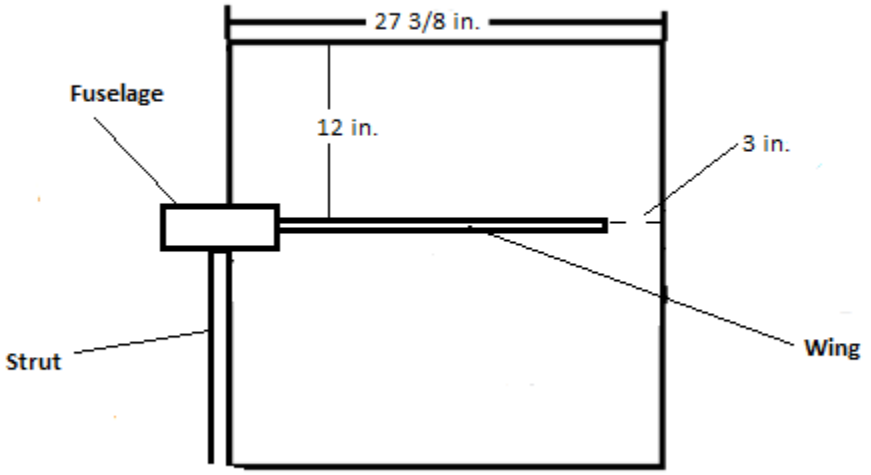

Figure 4.4: Drawing of swept wing test setup in open jet, flow direction out of the page

The deflections of both the leading and trailing edges of the wing were measured using a ruler. As with the unswept wing testing there were many sources of uncertainty, although the rod and clamp were not in the flow for the swept wing tests. The experimental results for the open-jet wind tunnel test are shown below. The airspeed and deflection are tabulated alongside the analytical results from the *Tornado* model. As before the effective change in the angle of attack was estimated based on equation (6), the expected change was -0.1 degrees from the set and expected 2 degrees angle of attack built into the model. Unlike the unswept model, due to the base plate dimensions, the swept wing model was exposed to the jet shear turbulence. The expected shear layer thickness at the tip of the swept wing was nearly 5 inches, placing at least 2 inches of the tip in the jet boundary.

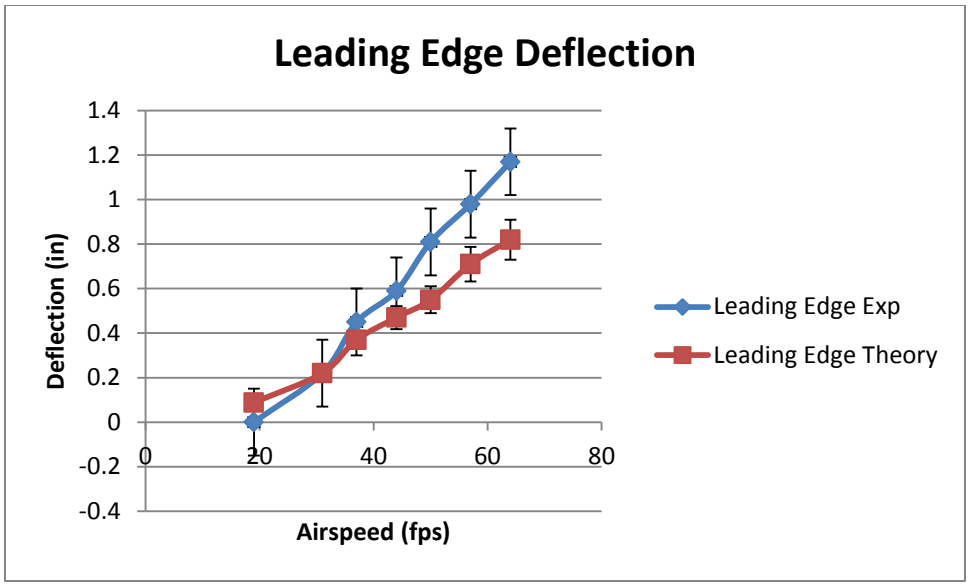

Figure 4.5: Leading edge deflection of test article in Open-Jet Tunnel

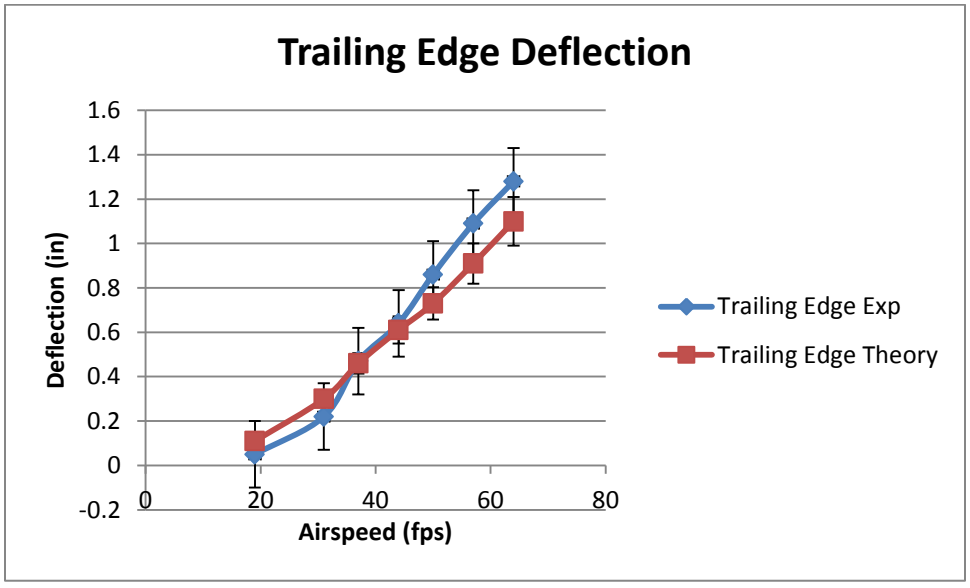

Figure 4.6: Trailing edge deflection of test article in Open-Jet Tunnel

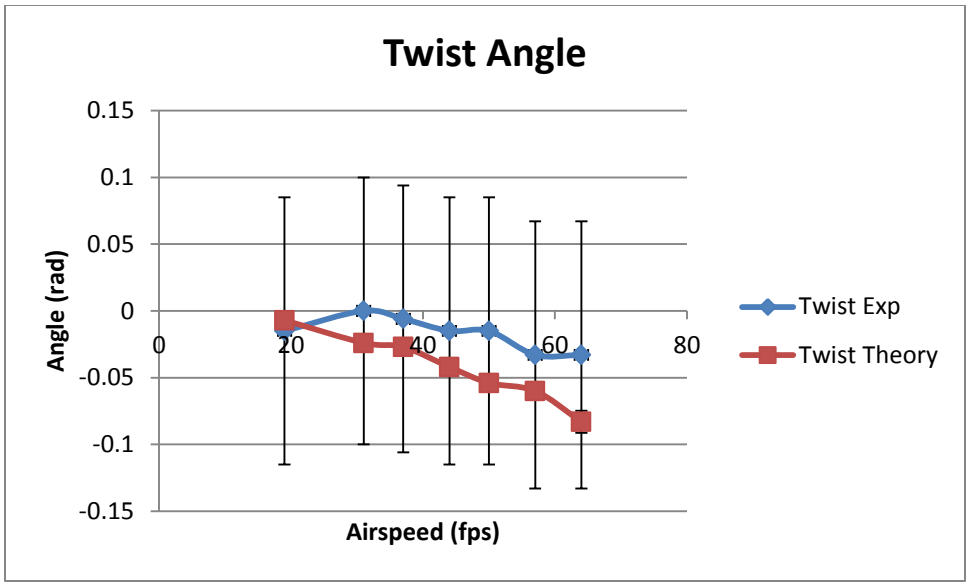

Figure 4.7: Wing twist angle of test article in Open-Jet Tunnel

In Figs. 4.5-7 the measured deflections for the leading and trailing edges, as well as the twist angle, are compared to the numerical model predictions. The error bars represent the uncertainties and wing tunnel effects applied to the measurements and model, which included the uncertainty of the ruler measurement as well as an error due to wing vibration, estimated at 0.1 inches. For the numerical model the only uncertainty was the wing stiffness. Despite the many uncertainties and the measurement error of the ruler the results measured in the open jet matched well with the theoretical results. There were some discrepancies due mostly to the difficulty of measurement; it is possible the wing tip oscillation, likely due to the tip exposure to the jet shear, caused the measurement difficulty. The wing oscillation was once again present and made the ruler measurements challenging. Luna Technologies Inc., was also represented at this test and took shape sensing measurements. Due to the wing oscillations no useful data was taken. Despite the data acquisition difficulties the shape sensing system functioned and the flexible wing test article performed as predicted by the numerical model.

The test article was then placed in the 6'x6' test section of the Virginia Tech Stability Wind Tunnel[10] by fixing the 2'x2' square aluminum panel base of the model in the floor of the test section. This wind tunnel is a continuous, single return, subsonic wind tunnel with a 24' long removable rectangular test section. The tunnel system is a closed loop but has an air exchange tower open to atmosphere for temperature stabilization. Downstream of the tower the flow is directed into a 18'x18' settling chamber with seven turbulence reducing screens. Flow exits the settling chamber and passes through a 9:1 contraction nozzle which accelerates the flow and further reduces turbulence. The turbulence levels in the stability tunnel are very low, less than 0.03% at 100 fps, and as such effects due to turbulence were ignored.

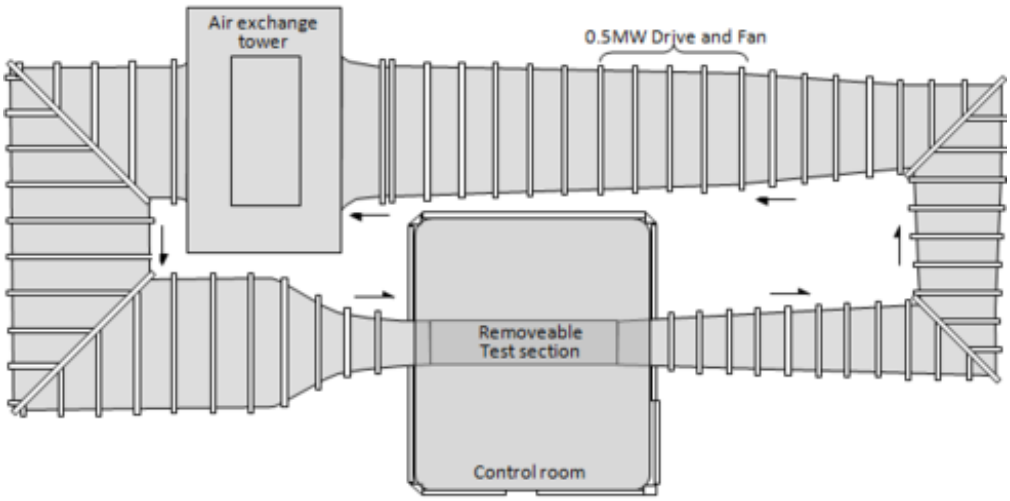

Figure 4.8: Virginia Tech Stability Wind Tunnel layout

On the starboard side the adjacent aluminum panel was replaced with a translucent plastic panel so that laser measurements could be made for deflection. A photograph of the setup is shown in Figure 4.7. The model was placed so that the tip of the right wing was 15 inches from the wall of the test section. This was done so that the wing would avoid the nearly 4 inch[11] boundary layer at the wall and be exposed only to free stream flow.

The theoretical model assumes the model is in free stream air without any surrounding boundaries. In a wind tunnel the flow is bound by walls, in the case of the Stability Wind Tunnel it is bound by four walls, one on each side. The presence of the wind tunnel model in the test section changes the flow field and causes predictable effects that would not be seen in a pure free stream environment. For the cases of this study only effects on lift are deemed important because the predominant factor causing the bending is the lifting force and the drag is ignored by the vortex lattice method. These boundaries produce changes in the effective angle of attack and dynamic pressure in the wind tunnel which both effectively increase the lift on the model.[12] In these cases the correction factors depended on ratios of the volume and lifting area of the test article relative to the total area of the test section. The correction in the effective velocity due to solid blockage is given in equation (8).

$$V = V_u(1 + \epsilon), \text{ where } \epsilon = 0.25\ (Model\ Fronal\ Area)/(Test\ section\ area) \qquad (8)$$

After consulting Harper and Pope the maximum effective change in velocity was found to be less than 0.2 feet per second, even at the highest airspeed. Using equation (7) the change in angle of attack due to downwash effects was calculated and the effective angle of attack change was 0.06 degrees. It should be noted that the form of the equation does not change for closed and open section wind tunnels, but the sign of the correction factor δ does. Due to the miniscule nature of these changes the wind tunnel effects were treated as negligible.

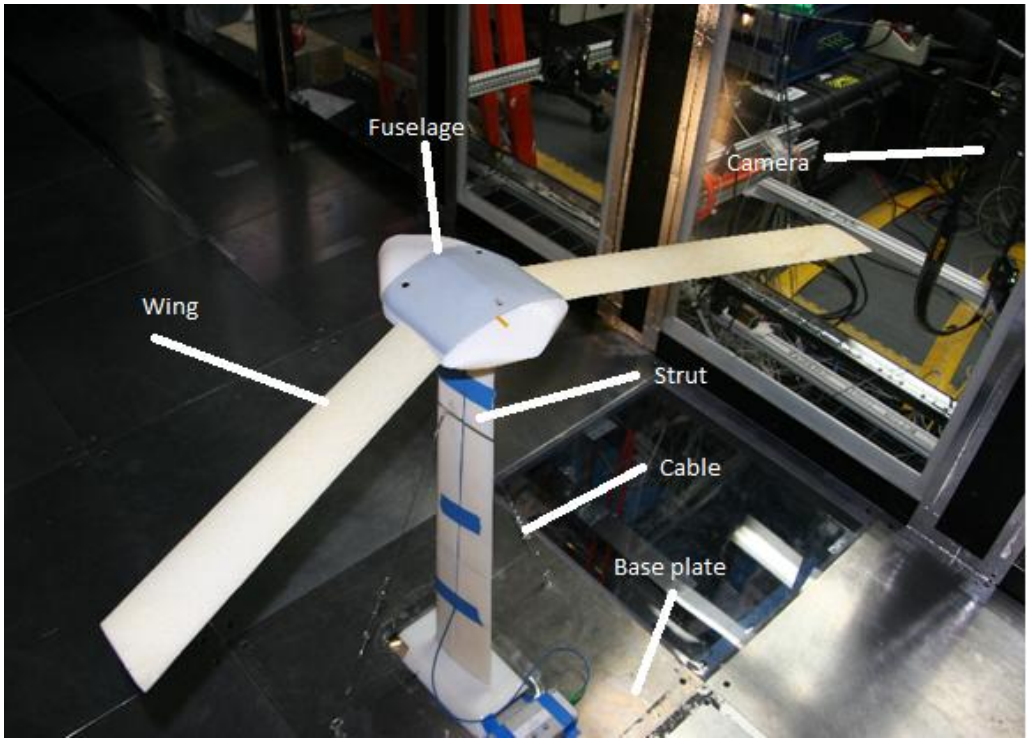

Figure 4.9: Stability wind tunnel set up

The stability wind tunnel was run at ascending airspeed from 16 – 95 fps in increments of about 7 fps. At each airspeed deflection measurements were recorded by the fiber optic system and laser device in order to capture wing deflection and twist. During data acquisition the shape sensing system showed signs of difficulty and after data processing it was discovered that no useful data had been taken. Photographs were also taken for displacement analysis by the grid system. The measured and predicted leading and trailing edge deflections as well as the twist angles at each airspeed are shown in Fig. 4.5-7 and the numerical results are shown in appendix 6.3. The uncertainties in each measurement are also shown in the form of error bars. The uncertainties in the theoretical predictions lay with the beam stiffness. As shown in appendices 6.1 and 6.2 the measured stiffness's varied by 20 percent.

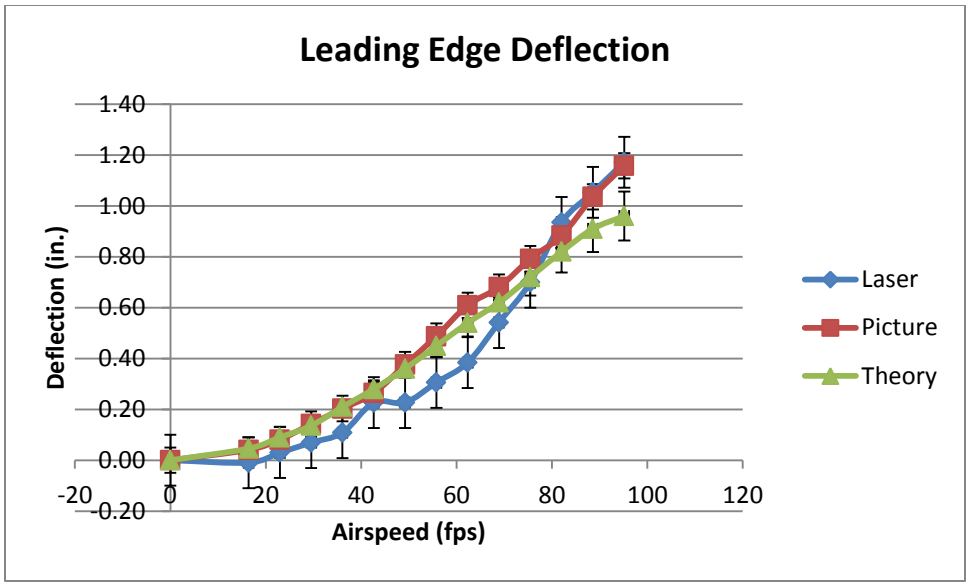

Figure 4.10: Leading edge deflection of test article in Stability Wind Tunnel

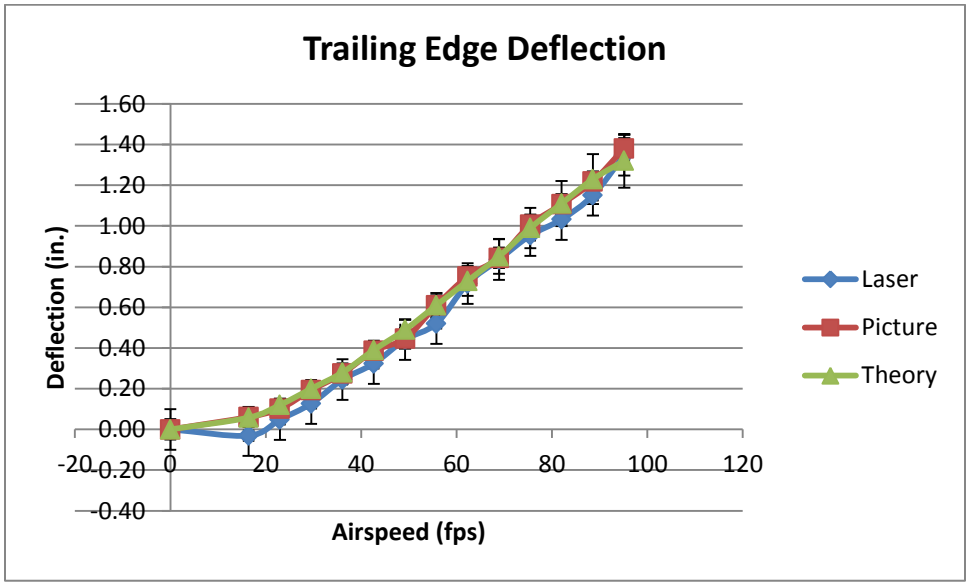

Figure 4.11: Trailing edge deflection of test article in Stability Wind Tunnel

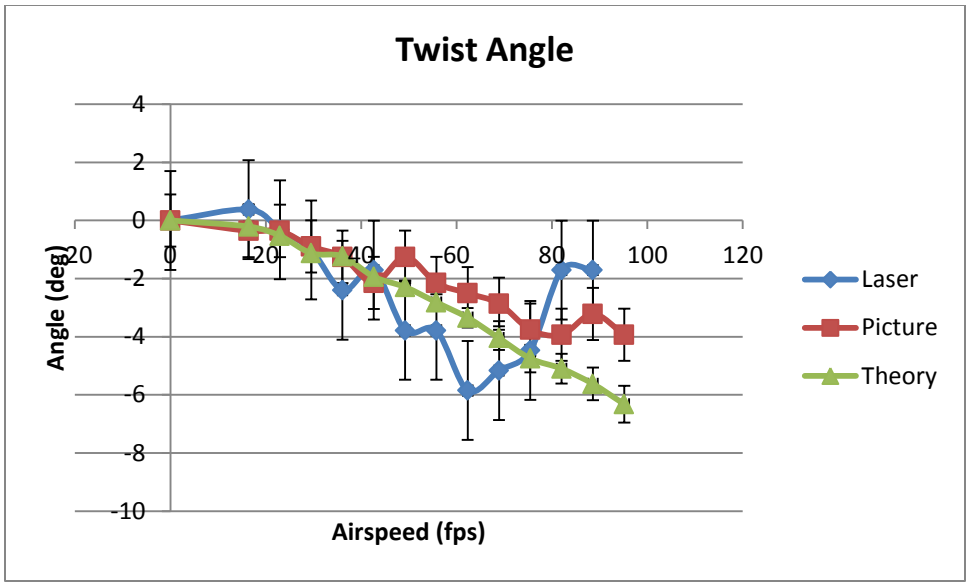

Figure 4.12: Wing twist angle of test article in Stability Wind Tunnel

In general the theoretical calculations agree with the measured results. As expected the flexible swept wing test article performed well in the wind environment. There are a few possible reasons for the observed disagreement between the experimental and numerically predicted results. The first is that the theoretical calculations ignore viscous effects, as well as thickness which are both drawbacks of the vortex lattice method. As shown in the previous section the uncertainty in the measurements may have also lead to error between the experimental and numerical results.

The largest discrepancies appear in the leading edge deflection measurements at high airspeeds. In most cases the deflection predicted by the theoretical model and the measured results differed by less than 10 %, while the twist less than 40 %.The largest disagreement in deflection between the analytical and experimental numbers is 17 % in the 95 fps case, while the largest twist discrepancy is 75 % at 89 fps. The percent change in twist may not be a very useful

calculation because of how small the angles that were measured are. Any small discrepancy causes a very large percentage difference change.

5 Conclusion

Flexible wing aircraft have the advantage of lower structural weight but are much more susceptible to flutter and free stream turbulence. In order to provide controls to account for these vulnerabilities information about the wing shape must be known. One such method of shape sensing is fiber optic sensors. These sensors use known light patterns in order to gauge the deflection and twist of the cable at a given time. Luna Innovations has developed such a system and in a joint research effort with Virginia Tech intended to demonstrate the systems applicability to aerospace interests. In order to accomplish this task a flexible wing test article was designed, modeled, constructed, and tested in order to validate the shape sensing system in a wind tunnel environment.

The mathematical modeling effort began with the expected loads on the wing as predicted by the VLM. The approximated load was then used to guide the design of a skinned foam core wing. The aeroelastic behavior of the design was then approximated by combining the loads calculated by the VLM with linear beam theories. A code was written to automate this process and iterate the geometry of the theoretical design as it deflected and twisted due to the approximated aerodynamic load. The code continued to iterate until a convergence criterion was satisfied and the wing geometry reached a steady state. The foam core wing was then constructed, and the stiffness properties were measured and then used in turn to update the theoretical model. A unswept wing wind tunnel model was first constructed in order to perform experimental tests, verify the theoretical calculations, and discover the practicality of different

manufacturing techniques. This effort revealed the capability of a simple foam core wing and fiberglass skin composite as an effective flexible wing test platform. This test article was then placed in the open-jet wind tunnel, and deflection measurements were taken at several airspeeds and angles of attack. The deflection results for the numerical model and experimental results matched well. It was apparent in both the experimental results and the theoretical model there was negligible twisting in the unswept wing.

Following the validation of the numerical model a full-span, swept-wing model was constructed. This test article was designed to house the fiber optic shape sensing system developed by Luna Technologies Inc., and to validate the system in a wind tunnel environment. After construction, half the span of the model was placed in the open-jet wind tunnel for a preliminary run at several airspeeds and at a fixed angle of attack of 2 degrees. The twist and deflection results for the open-jet experiment on the swept wing agreed with the theoretical model results. The model was then placed in the 6'x6' Virginia Tech Stability Wind Tunnel and again testing was run at 2 degrees angle of attack and various airspeeds. The deflection and twist of the test article wing were measured experimentally using photographs and using a laser displacement sensor. Once again the theoretical results agreed with the experimental results within margins of error and uncertainty.

From this study it is evident that simpler CAE methods, such as a VLM coupled with a linear beam theory, when applied correctly are useful design tools and provide relatively accurate approximations of the aeroelastics of flexible wings in steady flow conditions. In this case there was no commercial FEM or computationally taxing CFD used, all of the calculations were performed in Matlab. The static aeroelastic response predicted by the coupled structural and aerodynamic model compared with the experimental results showed little difference within the

expected error. In this regard the mathematical model combined with the experimental testing proved a useful tool for the aeroelastic analysis of flexible wings in low subsonic flow. The greatest advantage of using these simple methods is the small amount of time required for both coding and compiling. The theoretical model was not without its drawbacks however and consistently over predicted the twist observed in the experiments for the swept wing test article. This may have been due to airfoil thickness effects which *Tornado* does not account for. An additional pitfall of this analysis was the linear beam theory which did not account for shear deformation. In the future more robust methods could be used to further improve the calculations, and as computational power continues to improve more complex methods can be used with the same benefit of time. There are also steps that could be taken to make the experimental measurements more accurate such as a more consistent system for measurement of the leading edge deflection, especially for the laser distance finder. A method for measuring displacement distribution outside the shape sensing method could also be investigated.

The completed test article revealed that a flexible wing model for wind tunnel testing is a good platform for the aeroelastic testing of future shape sensing systems. In addition to the success of the mathematical methods the test article also performed as predicted. Although the shape sensing system was unable to acquire any useful shape data during the relatively short Stability Wind Tunnel experiment the system suffered no catastrophic failure and can be retested at a later date. However, this study highlighted some of the shortcomings of the shape sensing system. Wing vibrations pose an issue for the system measurement, which is an important hurdle for aerospace applications. It is possible that in the future, if the proper steps are taken in gearing the shape sensing system specifically for aerospace applications, that the fiber optic system will be an effective method for shape sensing.

References

[1] Houghton, E. L. and Carper, P.W. “Aerodynamics for Engineering Students, Fifth Edition” Butterworth-Heinemann 2003. pp. 337-341

[2] Moran, Jack. “An Introduction to Theoretical and Computational Aerodynamics,” John Wiley & Sons 1984.Dover publications 2003. pp. 129-134

[3] Melin, Thomas. “A Vortex Lattice MATLAB Implementation for Linear Aerodynamic Wing Applications,” Masters Thesis, Royal Institute of Technology. December 2000.

[4] Hjelmstad, Keith D. “Fundamentals of Structural Mechanics, Second Edition”. Springer Science + Business Media, Inc 2005. pp. 116-120

[5] “*Tornado*: Vortex Lattice Software”. Developed in cooperation between: KTH, Royal institute of Technology in Stockholm Sweden and University of Bristol, United Kingdom and the University of Linköping. download at: http://www.redhammer.se/*Tornado*/

[6] Beer, Ferdinand P. and Johnston, E. Russel Jr., “Mechanics of Materials, Second Edition,” Copyright McGraw-Hill 1992, 1981 McGraw-Hill Inc. pp. 164 & 716

[7] Timoshenko, S., “History of Strength of Materials”, McGraw-Hill New York 1953, Published 1983 Dover Publications, pages 28 and 334

[8] “0.7m Subsonic Open Jet Wind Tunnel, Facility Description” Virginia Polytechnic Institute and State University 2013. http://www.aoe.vt.edu/research/facilities/openjet.html

[9] Pankhurst, R. C., D. W. Holder, "Wind-Tunnel Technique: An Account of Experimental Methods in Low and High-Speed Wind Tunnels," Copyright London Sir Isaac Pitman & Sons LTD.

[10] "Virginia Tech Stability Wind Tunnel" Virginia Polytechnic Institute and State University 2013. http://www.aoe.vt.edu/research/facilities/stabilitytunnel/index.html

[11] Cred, E. D., "Aerodynamics and Acoustics of the Virginia Tech Stability Tunnel Anechoic System," Masters Thesis, Virginia Polytechnic Institute and State Univeristy. June 2008.

[12] Pope, A., Harper, J.J., "Low-Speed Wind Tunnel Testing," Copyright John Wiley & Sons Inc., New York | London | Sydney

[13] "Spiderwire, Products" Copyright 2013 Pure Fishing, Inc. http://www.spiderwire.com/cat.php

[14] Perry, B. III. Cole, S. R., Miller G. D., "Summary of an Active Flexible Wing Progam" Journal of Aircraft, Vol. 32, No.1, January – February 1995

[15] Creech, Gray. "Introducing the X-56 MUTT: Who Let the Dog Out?" NASA Dryden Flight Research Center. March 6th, 2012 http://www.nasa.gov/topics/aeronautics/features/x-56a_mutt.html

[16] Giallorenzi, T.R., Bucaro, J.A. et al. "Optical Fiber Sensor Technology" IEE Journal of Quantum Electronics, Vol. QE - 18, No.4, April 1982

[17] Mendex, Alex. **"**Medical Applications of Fiber-Optics: Optical Fiber Sees Growth as Medical Sensors". Laser Focus World. January 1st, 2011.

http://www.laserfocusworld.com/articles/2011/01/medical-applications-of-fiber-optics-optical-fiber-sees-growth-as-medical-sensors.html

[18] Uncredited. "Luna Fiber Optic Shape Sensing: Current State of Technology" Luna Innovations Incorporated. December 4th 2012. Document #: SS00021-D-TS. http://lunainc.com/wp-content/uploads/2012/08/SS-00021-D-TS_FiberOptic-Shape-Sensing-Snapshot+TechBackground_Rev002.pdf

[19] Bartels, R. E., Sayma, A. I., "Computational aeroelasticl modeling of airframes and turbomachinery: progress and challenges" Phil. Trans. R. Soc. A (2007)

[20] Eskandary, K., Dardel, M. et al, "Nonlinear aeroelastic analysis of high-aspect ratio wings in low subsonic flow" Acta Astronautica. August 2011

[21] Stragnac, T. W., Mook, D. T., "Numerical model of Unsteady Subsonic Aeroelastic Behavior" AIAA Journal Vol. 28, NO. 5, May 1990

[22] Bond, V. L., Canfield, R. A. et al, "Experimental Nonlinear Static Deflections of a Subscale Joined Wing". Journal of Aircraft Vol. 49 , No. 1, January – February 2012

[23] Wan, Z., Zhang, B. et al., "Static aeroelastic analysis of a high-aspect-ratio wing based on wind-tunnel experimental aerodynamic forces" Science China Vol. 54, No. 10 October 2011

[24] Martin, C. A. et al, "Design, Fabrication, and Testing of a Scaled Wind Tunnel Model for the Smart Wing Project". Journal of Intelligent Material Systems 2004 15: 269

[25] Carlsson, Martin, "Control Surface Response of a Blended Wing Body Aeroelastic Wind-Tunnel Model". Journal of Aircraft Vol. 42 , No. 3, May-June 2005

6 APPENDICES

6.1 Bending stiffness

In order to experimentally measure the bending stiffness of the test article static tip load testing was performed on a fixed bench top. This test involved placing stainless steel nuts of known weight on the tip of the wing and then measuring the displacement due to bending with a ruler. The model was fixed upside down making the washers easier to place as the wing had a relatively flat bottom surface. A photograph of the setup is shown in Fig A.1.

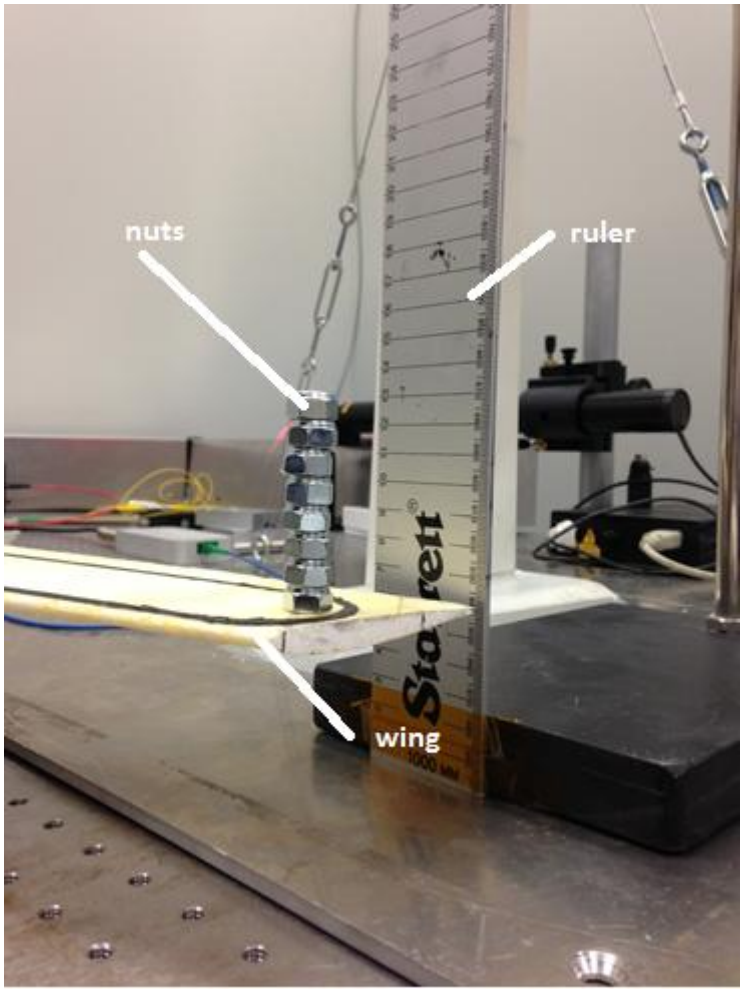

Figure 6.1: Photograph of bending stiffness test setup

The stiffness was calculated using equation (5) shown below. In this equation, *w* is the deflection, *P* the applied load, *L* the length of the wing and *EI* the stiffness.

$$w = \frac{PL^3}{3EI} \tag{9}$$

With the known force, wing length, and measured deflection the stiffness is easily calculated. Several weights were added and compared to ensure precision of the measurement. Below a plot showing the deflection against the tip load is given, the slope of the trend line is expected to be linear as the slope of the line should be constant due to constant length and stiffness.

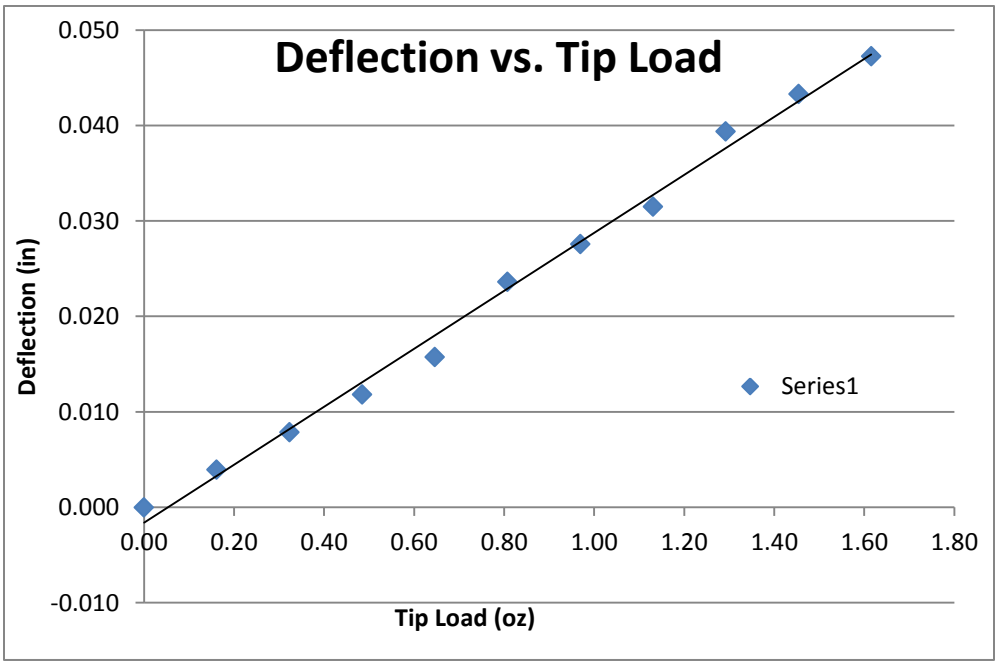

Figure 6.2: Plot of applied tip load vs. wing deflection for swept wing

Using the equation above the stiffness of the wing was calculated for each data point. The average stiffness was 396 lb-in^2 with a standard deviation of +/- 38 lb-in^2. This averaged stiffness was used to inform the theoretical model.

6.2 Torsional Stiffness and Shear Center Location

The shear center and torsional stiffness of the wing were experimentally measured using a single test. This test used a unswept wing section instead of the swept wing section and this was done for two reasons. The first was that the test would not have been able to decouple bending from twisting, and the second was the transformation performed to couple bending and twisting in the calculation takes place after the initial twist along the wing is found. This means that the torsional stiffness and shear center of the unswept wing are actually what is needed.

The test involved the placement of a balsa section on the wing tip, and attaching low stretch fishing line called *Spiderwire* [11] on either side of the wooden section. Weights were then hung from the string causing a measureable tension, this tension in the string caused the wings to twist and then twist and shear center measurements were made.

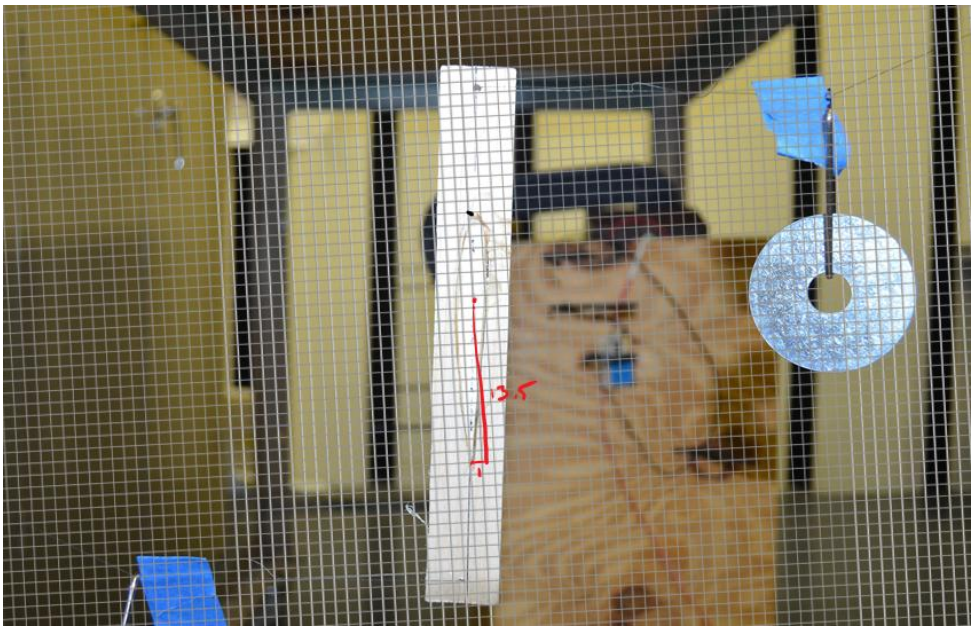

Figure 6.3: Picture of set up and grid measurement system.

The measurements made were made using photographs. At each measurement, a picture was taken and, by overlaying a grid, twist of the wing was measured. A sample picture is shown above. The twist was measured by comparing the chord line of the twisted wing with the un-weighted reference chord line. In order to determine the shear center, the intersection of these two lines was simply measured for each data point.

Table 6.1: Shear center location of swept wing airfoil section

Weight (lb)	# of grid squares	% chord
0.05734	6.5	33
0.101447	6.5	33
0.149966	7	35
0.198484	7.5	38
0.247002	8	40
0.29111	8	40
AVG	7.4	37

The shear center was measured at each applied load and the average location was used to inform the model. The average was calculated as 37% of the chord length, with a standard deviation of 3%. Because the measurement was made by counting the grid squares the uncertainty of the measurement is 0.5 grid squares.

The torsional stiffness of the wing was calculated using equation (1) where the length is known and the torque and twist are both measured. The twist was measured using the photographs and grid. The torque was calculated by measuring the angles in the strings and using the known weights to perform a nodal analysis in order to find the tension in the strings. Once the tension was known the torque was calculated by multiplying the tension by the moment arm for the tension in the strings about the shear center.

Table 6.2: Results of torsional stiffness static test for swept wing

Weight (lb)	Torque (in-lb)	Twist (rad)	Torsional Stiffness (lb-in^2)
0.05734	0.76728	negligible	N/A
0.101447	1.41692	0.058267	4.45E+02
0.149966	2.008886	0.073939	4.97E+02
0.198484	2.449681	0.09066	4.95E+02
0.247002	2.561598	0.113151	4.14E+02
0.29111	2.828684	0.12751	4.06E+02

The table above shows the results from the static twisting test. The average torsional stiffness came to 451 lb-in^2 with a standard deviation of 42 lb-in^2. The average value was used to inform the model.

6.3 Swept Wing Test Article Wind Tunnel Results

Table 6.3: Open-jet experimental results and analytical results for swept-wing

	Experimental Results			Analytical Results		
Airspeed (fps)	**LE Def. (in)**	**TE Def. (in)**	**Twist Angle**	**LE Def. (in)**	**TE Def. (in)**	**Twist Angle**
19	0.00	0.05	-0.015	0.088	0.11	-0.007
31	0.22	0.22	0.000	0.22	0.3	-0.024
37	0.45	0.47	-0.006	0.37	0.46	-0.027
44	0.59	0.64	-0.015	0.47	0.61	-0.042
50	0.81	0.86	-0.015	0.55	0.73	-0.054
57	0.98	1.09	-0.033	0.71	0.91	-0.060
64	1.17	1.28	-0.033	0.82	1.1	-0.083

Table 6.4: Wing deflection results for stability tunnel testing of swept wing model

	Deflection (in)					
Airspeed (fps)	**LE Las**	**TE Las**	**LE Pic**	**TE Pic**	**LE Theory**	**TE Theory**
0	0.00	0.00	0.00	0.00	0.00	0.00
16	-0.01	-0.03	0.04	0.06	0.05	0.06
23	0.03	0.05	0.08	0.10	0.09	0.12
30	0.07	0.13	0.14	0.19	0.14	0.20
36	0.11	0.24	0.20	0.27	0.21	0.28
43	0.23	0.32	0.26	0.39	0.28	0.39
49	0.23	0.44	0.38	0.45	0.36	0.49
56	0.31	0.52	0.49	0.61	0.45	0.61
62	0.38	0.72	0.61	0.75	0.54	0.73
69	0.54	0.84	0.68	0.84	0.62	0.85
75	0.70	0.95	0.79	1.01	0.72	0.99
82	0.94	1.03	0.88	1.11	0.82	1.11
89	1.05	1.15	1.04	1.22	0.91	1.23
95	1.17	1.35	1.16	1.38	0.96	1.32

6.4 Sample Code

A sample of the code used to estimate wing deflection and twist is given here. This includes sample geometry and state *structs* as well as all of the subfunctions written by Virginia Tech that the main program calls. All of the *Tornado* subfunctions used can be found at their website: http://www.redhammer.se/*Tornado*/.

```
clear all,close all,clc
% Initial Inputs
results=[];
settings=config('startup');
m=1; % #number of wings (doesn't change
n=23; % #of semi-spanwise partisionschanged during iteration
% ^one will note that there are n-4 terms everywhere, this is because
% there are n-4 partitions on the wings, 4 partitions are used by the
fuselage
% and i am only intereste n flexing the wing.

% material properties (metric)
E=4*10^6;
GJ=1.3;
Icomp=2.84*(10^-7);
span=0.5334;
chord=0.2794;
cfoil=0.0762;

%geometry
flapped=0+zeros(m,n); % is the wing flapped? (1 yes, 0 no)
nwing=m; %number of wings
nelem=n+zeros(1,m); %number of spanwise partitions
CG=[0 0 0]; %location of cg (irrelevant)
ref_point=CG; % reference point for forces and panel loactions
symetric=1+zeros(1,n); % is wing symmetric about x axis? (1 yes, 0 no)
startx=0+zeros(1,n); % these three describe where the wing is positioned
starty=0+zeros(1,n);
startz=0+zeros(1,n);
c=chord+zeros(1,n); %root chord length m
foil=cell(m,n,2); % type of airfoil (cell format)
foil(:,:,1)=java.lang.String('2410'); %type of airfoil at root
foil(:,1,1)=java.lang.String('0027'); %for fuselage
foil(:,2,1)=java.lang.String('0027');
foil(:,3,1)=java.lang.String('0027');
foil(:,4,1)=java.lang.String('0027');
foil(:,:,2)=java.lang.String('2410'); %type of airfoil at tip
foil(:,1,2)=java.lang.String('0027');
foil(:,2,2)=java.lang.String('0027');
foil(:,3,2)=java.lang.String('0027');
nx=8+zeros(m,n); %number of panels chordwise
```

```
TW=zeros(m,n,2);
TW(:,:,1)=0; % inboard twist of partition
TW(:,:,2)=0; % outboard twist of partition
dihed=0+zeros(m,n);
ny=1+zeros(m,n); %number of semi spanwise panels
b=span/n+zeros(m,n); % half span m
T=1+zeros(m,n); %taper ratio
T(m,1)=0.99; %tapers for fuselage partitions
T(m,2)=0.88;
T(m,3)=0.72;
T(m,4)=0.44;
SW=22*pi/180+zeros(m,n); % sweep matrix
SW(1)=0; %tsweeps for fuselage partitions
SW(2)=0.7854;
SW(3)=0.7854;
SW(4)=0.7854;
meshtype=1+zeros(m,n); %choose half cosine mesh type
fc=0+zeros(m,n); % next three are for for flaps (ignore)
fnx=0+zeros(m,n);
fsym=0+zeros(m,n);
flap_vector=0+zeros(m,n);

%state
AS=29;  % airspeed in m/s
alpha=2*pi/180; % AOA in radians
betha=0;    % sideslip angle
P=0;  % roll angular velocity rad/s
Q=0;    % pitch angular velocity
R=0;    % yaw angular velocity
alphadot=0; % rate of change of AOA
bethadot=0; % rate of change of sideslip angle
ALT=0; % altitude
rho=1.186; % air density in tunnel
pgcorr=0;   % use prandtl-glauert correction? (1 yes, 0 no)
adot=0; % need these...
bdot=0;

%Begin
%Set Up geometry (struct)
geoin=struct('flapped',flapped,'nwing',nwing,'nelem',nelem,'CG',CG,'ref_point
',ref_point,'symetric',symetric,'startx',startx,'starty',starty,'startz',star
tz,'c',c,'foil',{foil},'nx',nx,'TW',TW,'dihed',dihed,'ny',ny,'b',b,'T',T,'SW'
,SW,'meshtype',meshtype,'fc',fc,'fnx',fnx,'fsym',fsym,'flap_vector',flap_vect
or);

%Set up state (struct) **THIS DOES NOT CHANGE**
state=struct('AS',AS,'alpha',alpha,'betha',betha,'P',P,'Q',Q,'R',R,'alphadot'
,alphadot,'bethadot',bethadot,'ALT',ALT,'rho',rho,'pgcorr',pgcorr,'adot',adot
,'bdot',bdot);

JID='batchjob';
% Get results for initial geometry and state
[lattice,ref]=fLattice_setup2(geoin,state,0); %create lattice

solverloop5(results,1,JID,lattice,state,geoin,ref); % process results
```

```
cd(settings.odir)
    load batchjob-Cx;
cd(settings.hdir)

%this part makes sure only the wing geometry is iterated
        j=1;
    for i=1:length(results.ystation)
        if results.ystation(i)>0.09
            yst(j)=results.ystation(i);
            BMom(j)=results.BendingMoment(i);
            j=j+1;
        else
        end
    end
    j=1;
    for i=1:length(results.M(:,1))
        if lattice.COLLOC(i,2)>0.09
            colloc(j,:)=lattice.COLLOC(i,:);
            TMom(j,:)=results.M(i,:);
            j=j+1;
        else
        end

    end
%Calculate deflection and iterate geometry
[w,dw,tw,rtstressnc,tipdef,eal]=NACA2410def(n,cfoil,state.AS,state.rho,geoin.
T,geoin.b,E,Icomp,yst,results.ystation,BMom,results.ForcePerMeter,colloc,TMom
,GJ);

g=linspace(0,geoin.b(1,1)*(n-4),n-4); % 10 stations on half span (for plot)

last=0;


%(***NOTE: BENDING SHOULD NOT CHANGE LOAD ON WING MUCH ONLY TWIST SHOULD****)

while (abs((w(end)-last)))/(last)>0.005

    last=w(end);
    oldaero=results.BendingMoment;
    oldload=results.F;


    % change span

    goal=0;
    i=1;
    while goal<0.43815
        i=i+1;
        temp=sqrt((w(i)-w(i-1))^2+(g(i)-g(i-1))^2);
        goal=goal+temp;
    end

    newspan=g(i);
```

```
    %iterate geometry
    nwing=m;
    nelem=n+zeros(1,m);
    symetric=1+zeros(1,n);
    startx=0+zeros(1,n);
    starty=0+zeros(1,n);
    startz=0+zeros(1,n);
    c=chord+zeros(1,n);
    foil=cell(m,n,2); % type of airfoil (cell format)
    foil(:,:,1)=java.lang.String('2410'); %type of airfoil at root
    foil(:,1,1)=java.lang.String('0027');
    foil(:,2,1)=java.lang.String('0027');
    foil(:,3,1)=java.lang.String('0027');
    foil(:,4,1)=java.lang.String('0027');
    foil(:,:,2)=java.lang.String('2410'); %type of airfoil at tip
    foil(:,1,2)=java.lang.String('0027');
    foil(:,2,2)=java.lang.String('0027');
    foil(:,3,2)=java.lang.String('0027');
    nx=8+zeros(nwing,nelem); %number of panels chordwise

    TW=zeros(m,n,2);
    dihed=zeros(m,n);
    TW(m,1,1)=0;
    dihed(1)=0;
    for i=6:n
          TW(m,i,1)=tw(i-5); % inboard twist of partition
          TW(m,i,2)=tw(i-4); % outboard twist of partition
          dihed(i)=dw(i-4);
    end

    ny=1+zeros(m,n); %number of semi spanwise panels
    b=(0.09525+newspan)/n+zeros(m,n); % half span m
    T=1+zeros(m,n); %taper ratio
    T(m,1)=0.99; %tapers for fuselage partitions
    T(m,2)=0.88;
    T(m,3)=0.72;
    T(m,4)=0.44;
    SW=22*pi/180+zeros(m,n); % sweep matrix
    SW(1)=0; %tsweeps for fuselage partitions
    SW(2)=0.7854;
    SW(3)=0.7854;
    SW(4)=1.1;
    meshtype=1+zeros(m,n); %choose half cosine mesh type
    flapped=zeros(m,n);
    fc=zeros(m,n); % next three are for for flaps (ignore)
    fnx=zeros(m,n);
    fsym=zeros(m,n);
    flap_vector=zeros(m,n);


    %Set Up new geometry (struct)

geo=struct('flapped',flapped,'nwing',nwing,'nelem',nelem,'CG',CG,'ref_point',
ref_point,'symetric',symetric,'startx',startx,'starty',starty,'startz',startz
,'c',c,'foil',{foil},'nx',nx,'TW',TW,'dihed',dihed,'ny',ny,'b',b,'T',T,'SW',S
```

```
W,'meshtype',meshtype,'fc',fc,'fnx',fnx,'fsym',fsym,'flap_vector',flap_vector
);

    JID='batchjob';
    % Get results for new geometry
    [lattice,ref]=fLattice_setup2(geo,state,0); %create lattice

    solverloop5(results,1,JID,lattice,state,geo,ref); % process results

    cd(settings.odir)
        load batchjob-Cx;
    cd(settings.hdir)

    % relax load
    results.BendingMoment=results.BendingMoment-0.7*abs(oldaero-
results.BendingMoment);

        j=1;
    for i=1:length(results.ystation)
        if results.ystation(i)>0.09
            yst(j)=results.ystation(i);
            BMom(j)=results.BendingMoment(i);
            j=j+1;
        else
        end
    end
    j=1;
    for i=1:length(results.M(:,1))
        if lattice.COLLOC(i,2)>0.09
            colloc(j,:)=lattice.COLLOC(i,:);
            TMom(j,:)=results.M(i,:);
            j=j+1;
        else
        end

    end

    % compute new deflection

[w,dw,tw,rtstressnc,tipdef,eal]=NACA2410def(n,cfoil,state.AS,state.rho,geoin.
T,geoin.b,E,Icomp,yst,results.ystation,BMom,results.ForcePerMeter,colloc,TMom
,GJ);


end


    wTE=39.3701*(w-(chord-eal)*sin(tw));
    wLE=(w+eal*sin(tw))*39.3701;
    figure(3)
    plot(g*39.3701,wLE,'k') %convert to inches
    hold on
    plot(g*39.3701,wTE)
    legend('Leading Edge','Trailing Edge')
    title('Deflection')
```

```
    ylabel('Deflection (in)')
    xlabel('y (in)')

    tipdefperc=100*tipdef/17.25
    Leading=wLE(end)
    Trailing=wTE(end)

function[w,dw,tw,rtstressnc,tipdef,eal]=NACA2410def(n,c0,Ue,rho,r,span,E,Icom
p,yst,ystato,Bmvec,Lift,colloc,M,GJ)

    %dynamic pressure
    qden=.5*rho*Ue^2;

    %Airfoil Points
    figure(1)
    [yp,xp]=NACA4shape(2,4,10,1); %for NACA 2410

    g=linspace(0,span(1,1)*n,n-4); % 10 stations on half span

    syms d

    %MOI Using written function
    [Ivec,Ifun]=ryanmm1_taperMOI_fun(xp,yp,r(1,8),c0,span(1,1)*n,3,n);
    Ivec=Ivec+Icomp;

    %Lift load
    figure(2)
    plot(ystato*39.3701,Lift*(39.3701/4.44822))
    title('Lift Along Span')
    xlabel('Span (in)')
    ylabel('Lift Load (lb/in)')
    hold on
%
[q,chords,liftvec]=liftload_fun(yst,CL,7,span(1,1)*n,c0(1,1),r(1,1),qden);

%     %Shear
%     EIw3=int(q,d);
%     EIw3=EIw3-int(q,d,0,span(1,1)*n);
% %     figure(4)
% %     plot(g,subs(EIw3,d,g))
% %     title('Shear')
% %     ylabel('-Shear (N)')
% %     xlabel('x (m)')
%
%     %Moment
%     EIw2=int(EIw3,d);
%     EIw2=EIw2-int(EIw3,d,0,span(1,1)*n);
% %     figure(5)
% %     plot(g,subs(EIw2,d,g))
% %     title('Moment')
% %     ylabel('-Moment (N.m)')
% %     xlabel('x (m)')
%
%     %make moment vector for iterative integration
%     for hj=2:length(g)
```

```
%          avg=(g(hj)+g(hj-1))/2;
%          Mvec(hj)=subs(EIw2,d,avg);
%      end

    %Angle
    Mvec=-Bmvec;
    angsum=0;
    Ew1=0;
    for count=2:length(Mvec)
        temp(count)=(Mvec(count)/Ivec(count))*(span(1,1)*(n-4)/length(Mvec));
        angsum=angsum+temp(count);
        Ew1(count)=angsum;
    end
    dw=Ew1./E;
    %DEFLECTION
    sumdef=0;
    Ew=0;
    for count=1:length(Ew1)
        tempd(count)=Ew1(count)*(span(1,1)*(n-4)/length(Ew1));
        sumdef=sumdef+tempd(count);
        Ew(count)=sumdef;
    end
    w=Ew./E;

    eal=c0*0.37; % approximate torsion model as ellipse

    % produce moment vector. M= r x F
    Mpan1=cosd(22)*M(:,2);% the angle here is to transfer to swept
    Mpan2=-sind(22)*M(:,1); %coordinate system
    Mpan=Mpan1+Mpan2;

    for i=1:length(g)
            %use 8 because there are 8 chordwise panels
        Mstat(i)=sum(Mpan(8*(i-1)+1):Mpan(8*i));
        ystat(i)=colloc(8*i,2);
    end
    [torq]=distrbload_fun(ystat,Mstat,span(1,1)*n,6,(n-4));

    tw=0;
    sumtwist=0;
    %TWIST
    for count=1:length(torq)
        tempt=(torq(count)/GJ)*(span(1,1)*n/length(torq));
        sumtwist=sumtwist+tempt;
        tw(count)=sumtwist;
    end
    tw=atan(cosd(22)*tan(tw)-sind(22)*sin(dw));
    %other outputs
    tipdef=w(length(g))*39.3701;
    rtstressnc=c0*0.1*Mvec(2)/Ivec(2);

end


function [Itap,Ifun] = ryanmm1_taperMOI_fun(xp,yp,r,c0,span,n,gol)
```

```
%%%%% Inputs
%xp: xpoints of airfoil cross section
%yp: ypoints of airfoil cross section
%r: taper ratio
%c0: root chord
%span: length of one wing
%n: order of polynomial to match function to (n=4 suffices)

%%%%% Outputs
%Ifun: approximating MOI function, in terms of distance "d"
%Itap: vector of cross sectional MOI values along span
%
    g=linspace(0,span,gol);

    c=(r-1)*c0.*g./span+c0;

% MOI
     for count=1:length(g) %creat Ivec at 100 points along span
        xpt=c(count)*xp;
        ypt=c(count)*yp;
        I(count)=0;
        for j=2:length(xp)
            Itemp=0;
            for i=2:length(yp)
                Itemp1=0.5*(ypt(i)^2+ypt(i-1)^2)*abs(ypt(i)-ypt(i-1));
                Itemp=Itemp+Itemp1;
            end
            Itemp=Itemp*abs(xpt(i)-xpt(i-1));
            I(count)=I(count)+Itemp;
        end
     end
    f=polyfit(g,I,n); %create function
    syms d
    Ifun=0;
    for k=1:n+1
        Ift=f(k)*d^((n+1)-k);
        Ifun=Ifun+Ift;
    end
    for hj=2:length(g) %use function to estimate midpoints
        avg=(g(hj)+g(hj-1))/2;
        Itap(hj)=subs(Ifun,d,avg);
    end
%     figure(1)
%     plot(xp,yp)
%     title('airfoil shape')
%     figure(2)
%     plot(g,I) %(for comparison)
%     hold on
%     plot(g,subs(Ifun,d,g),'r')
%     title('MOI comparison')
%     ylabel('MOI (m^4)')
%     xlabel('x (m)')
End

function [ypts,xpts]=NACA4shape(a,b,cd,chord)
tmax=cd/100;
```

```
xcmax=b/10;
cmax=a/100;
xptsc=linspace(0,1);
yt=(tmax/.2)*chord*(0.2969*sqrt(xptsc)-0.1260*xptsc-
0.3516*xptsc.^2+0.2843*xptsc.^3-0.1015*xptsc.^4);
    for i=1:length(xptsc)
        if xptsc(i)<xcmax
            yc(i)=(cmax*xptsc(i)/(xcmax^2))*(2*xcmax-xptsc(i));
        else
            yc(i)=(cmax*(1-xptsc(i))/((1-xcmax)^2))*(1-2*xcmax+xptsc(i));
        end
    end
    xupper(1)=0;
    yupper(1)=0;
    xlower(1)=0;
    ylower(1)=0;
    for i=2:length(yc)
        theta(i)=atan((yc(i)-yc(i-1))/(xptsc(i)-xptsc(i-1)));
        xupper(i)=xptsc(i)-yt(i)*sin(theta(i));
        xlower(i)=xptsc(i)+yt(i)*sin(theta(i));
        yupper(i)=yc(i)+yt(i)*cos(theta(i));
        ylower(i)=yc(i)-yt(i)*cos(theta(i));
    end
    for i=1:length(xlower)
       xlower1(i)=xlower(length(xlower)-(i-1));
       ylower1(i)=ylower(length(xlower)-(i-1));
    end
    xupper(end)=1;
    xlower1(end)=[];
    xlower1(1)=1;
    xpts=chord*[xlower1';xupper'];
    ylower1(end)=[];
    ylower1(1)=0;
    yupper(end)=0;
    ypts=chord*[ylower1';yupper'];
    plot(xpts,ypts)
    title('Airfoil Shape')
    axis([chord-2*chord 3*chord -chord chord])
end

function [torq]=distrbload_fun(x,F,span,n,gol)
    g=linspace(0,span,gol);
    f=polyfit(x,F,n);
    syms d
    Lfun=0;
    for k=1:n+1
        Lft=f(k)*d^((n+1)-k);
        Lfun=Lfun+Lft;
    end
    for hj=2:length(g)
        avg=(g(hj)+g(hj-1))/2;
        torq(hj)=subs(Lfun,d,avg);
    end
end
```